



HAL
open science

Substrate stiffness impacts early biofilm formation by modulating *Pseudomonas aeruginosa* twitching motility

Sofia Gomez Ho, Lionel Bureau, Karin John, Delphine Débarre, Sigolène Lecuyer

► To cite this version:

Sofia Gomez Ho, Lionel Bureau, Karin John, Delphine Débarre, Sigolène Lecuyer. Substrate stiffness impacts early biofilm formation by modulating *Pseudomonas aeruginosa* twitching motility. *eLife*, 2023, 10.1101/2022.02.18.480999 . hal-03798581v2

HAL Id: hal-03798581

<https://hal.science/hal-03798581v2>

Submitted on 10 May 2023

HAL is a multi-disciplinary open access archive for the deposit and dissemination of scientific research documents, whether they are published or not. The documents may come from teaching and research institutions in France or abroad, or from public or private research centers.

L'archive ouverte pluridisciplinaire **HAL**, est destinée au dépôt et à la diffusion de documents scientifiques de niveau recherche, publiés ou non, émanant des établissements d'enseignement et de recherche français ou étrangers, des laboratoires publics ou privés.

1 Substrate stiffness impacts early 2 biofilm formation by modulating 3 *Pseudomonas aeruginosa* twitching 4 motility

5 Sofia Gomez², Lionel Bureau², Karin John², Elise-Noëlle Chêne¹, Delphine
6 Débarre^{2*}, Sigolène Lecuyer^{1,2*}

*For correspondence:

[delphine.debarre@](mailto:delphine.debarre@univ-grenoble-alpes.fr)

univ-grenoble-alpes.fr (DD);

sigolene.lecuyer@ens-lyon.fr (SL)

7 ¹Université Lyon, ENS de Lyon, Université Claude Bernard, CNRS, Laboratoire de
8 Physique, F-69342, Lyon, France; ²Université Grenoble Alpes, CNRS, LIPhy, 38000
9 Grenoble, France

10

11 **Abstract** Surface-associated lifestyles dominate in the bacterial world. Large multicellular
12 assemblies, called biofilms, are essential to the survival of bacteria in harsh environments, and
13 are closely linked to antibiotic resistance in pathogenic strains. Biofilms stem from the surface
14 colonization of a wide variety of substrates encountered by bacteria, from living tissues to inert
15 materials. Here, we demonstrate experimentally that the promiscuous opportunistic pathogen
16 *Pseudomonas aeruginosa* explores substrates differently based on their rigidity, leading to striking
17 variations in biofilm structure, exopolysaccharides (EPS) distribution, strain mixing during
18 co-colonization and phenotypic expression. Using simple kinetic models, we show that these
19 phenotypes arise through a mechanical interaction between the elasticity of the substrate and
20 the type IV pilus (T4P) machinery, that mediates the surface-based motility called twitching.
21 Together, our findings reveal a new role for substrate softness in the spatial organization of
22 bacteria in complex microenvironments, with far-reaching consequences on efficient biofilm
23 formation.

24

25 Introduction

26 The transition of bacteria from a planktonic to a surface-attached state is of paramount importance
27 in biofilm formation. In consequence, the way bacteria sense and respond to the close proximity
28 of a surface has been the subject of intense scrutiny (*Dufrêne and Persat, 2020; Laventie and Je-*
29 *nal, 2020*). This interaction involves different aspects of bacterial motility: swimming towards the
30 surface, but also swarming, gliding or twitching that are used by attached bacteria to explore the
31 surface collectively or individually (*Wadhwa and Berg, 2022; Conrad et al., 2011*). Eventually, per-
32 manent bacterial adhesion and microcolony structuration may arise, through mechanisms which
33 essential ingredients are known (production of matrix, loss of motility), but in response to cues
34 that remain unclear.

35 Bacteria are ubiquitous and can successfully colonize a wide range of biological tissues and
36 abiotic surfaces (*Stoodley et al., 2002; Mann and Wozniak, 2012*). Different environments often re-
37 sult in different phenotypes for a given microorganism (*Dötsch et al., 2012; Cornforth et al., 2018*).
38 However, although chemical signaling has long been known to impact bacterial gene regulation,
39 it remains unclear how the mechanical properties of the encountered surface might impact bac-

40 terial behavior (*Persat et al., 2015b*). In this paper, we investigate how the rigidity of a substrate
41 modifies bacterial motility, and by doing so impacts microcolony morphogenesis and early biofilm
42 development.

43 *Pseudomonas aeruginosa* (PA) is an opportunistic rod-shaped pathogen that contaminates a
44 wide range of substrates, from very soft tissues to rigid implants (*Moradali et al., 2017; Chang,*
45 *2018*). A particularly gifted and versatile biofilm-former, it is extremely prone to developing antibi-
46 otic resistance (*Pang et al., 2019; Boucher et al., 2009*). PA has developed an arsenal of techniques
47 to move on surfaces: among them is twitching motility, that allows single bacteria to translocate
48 across surfaces using type IV pili (T4P) (*Maier and Wong, 2015*). T4P are thin protein filaments on
49 the bacterial surface that can extend and contract by assembly and disassembly of the protein
50 subunit PilA. The tip of T4P acts as a promiscuous hook that can grasp most surfaces. Attachment,
51 contraction, detachment and extension cycles propel bacteria (*Merz et al., 2000; Maier and Wong,*
52 *2015; Skerker and Berg, 2001; Talà et al., 2019*). This surface motility is important for bacteria to effi-
53 ciently settle on surfaces, but the exact mechanisms at play are unknown (*O'Toole and Kolter, 1998;*
54 *Leighton et al., 2015; Craig et al., 2019*). The function of T4P and the fact that it exerts forces on
55 its environment make it an obvious candidate for surface-sensing mechanisms (*Merz et al., 2000;*
56 *Dufrêne, 2015; Sahoo et al., 2016*). Recent results have shown that the polar localization of pili in
57 PA could happen in response to surface-sensing (*Cowles and Gitai, 2010*). Polarly-localized pili lead
58 to persistent rather than random displacements, as well as specific effects such as the upstream
59 migration of bacteria submitted to strong flows (*Shen et al., 2012*). Reversal of twitching bacteria is
60 rapidly induced upon meeting obstacles, suggesting a mechanical feedback from T4P (*Kühn et al.,*
61 *2021*). In addition, PA can exert different types of virulence, from acute attacks to chronic infec-
62 tions (*Furukawa et al., 2006; Valentini and Filloux, 2016*), and specific host-pathogen interactions
63 have traditionally been considered as the key players in the regulation of these virulence pathways
64 (*Gellatly and Hancock, 2013*). However, surface-sensing in itself has recently appeared as a poten-
65 tial signal that could trigger the upregulation of virulence-associated genes (*Islam and Krachler,*
66 *2016; Persat et al., 2015a; Siryaporn et al., 2014*). Although the global effect of surface rigidity on
67 bacterial adhesion and biofilm formation has sometimes been addressed (*Saha et al., 2013; Song*
68 *and Ren, 2014; Song et al., 2018a*), so far how the micromechanical environment experienced by
69 individual bacteria impacts their behavior is still unclear, possibly because of the difficulty to de-
70 sign and control microenvironments that allow for a fine tuning of mechanical properties at the
71 bacterial scale, along with negligible changes of the chemical environment.

72 In this study, we use a home-designed microfluidic setup to investigate at the single-cell level
73 the influence of substrate rigidity on PA bacteria adhering to an open surface, under controlled flow
74 conditions. We first demonstrate that substrate elasticity strongly impacts early microcolony de-
75 velopment. Focusing on single-cell behaviour, we then study quantitatively how rigidity modulates
76 bacterial motility and propose a purely mechanistic model to account for our observations. Fi-
77 nally, we demonstrate that this mechanical tuning of the motility explains rigidity-induced changes
78 in early surface colonization: we explore its consequences in terms of microcolony morphology,
79 matrix deposition, strain mixing and long-term gene expression.

80 Results

81 In order to explore *in situ* the effect of substrate rigidity on the behavior of adhering bacteria, we
82 have developed an experimental approach to include mechanically well-defined hydrogel pads in
83 a microfluidic channel providing controlled flow conditions and allowing confocal imaging (Fig. 1A).
84 We use the biocompatible hydrogel polyacrylamide (PAA), which has been extensively used to in-
85 vestigate cell-substrate interaction and mechanotransduction in mammalian cells. By varying the
86 amount of bisacrylamide cross-linker during its preparation, PAA can span a biologically-relevant
87 range of rigidities (from ~ 1 to 100 kPa) while keeping a low viscous dissipation. Several pads, with
88 different's modulus values ranging from ~ 3 to 100 kPa (see Fig.1-fig. suppl. 1, and Methods and
89 Materials), are used in each single experiment, and bacteria adhering on PAA and glass surfaces

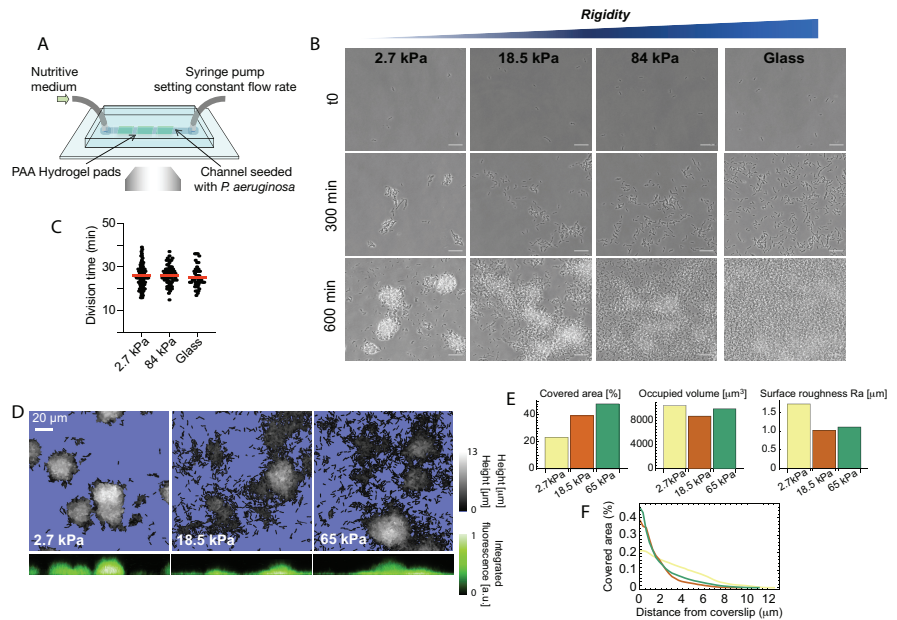


Figure 1. Bacterial microcolony formation depends on substrate rigidity. (A) Experimental setup: bacteria (*P. aeruginosa* strain PAO1) are imaged in a flow cell under constant flow of minimal medium. (B) After 10h, dense, isolated colonies form on soft PAA (2.7 kPa) while bacteria are more evenly distributed on stiff PAA (84 kPa), closer to what is observed on glass. Scale bars, 20 μm . (C) Bacterial growth is not impacted by substrate rigidity. (D) 3D reconstruction of colonies confirms their hemispherical shape on soft substrates. (E) Surface coverage is lower on soft substrates, but total volume of colonies is conserved, with a higher roughness value. (F) Fraction of area occupied by the bacteria as a function of the distance from the coverslip, showing flatter colonies on rigid substrates.

90 are imaged with high-resolution phase-contrast and fluorescence time-lapse imaging, from very
 91 low surface coverage up to the formation of microcolonies (1 frame/min over ~ 10 hours).

92 **Substrate elasticity modifies bacterial colonization of PAA in a T4P-dependent man-**
 93 **ner**

94 We first focus on the effect of substrate rigidity on early microcolony formation. Straightforward
 95 observations with phase-contrast imaging show a striking impact on the shape of microcolonies
 96 after a few hours (Fig. 1B and Video 1): on the softest hydrogels (< 10 kPa), bacteria form well-
 97 defined, dense hemispherical colonies; in contrast, on stiff hydrogels, bacteria are distributed in
 98 a thin layer covering most of the surface, a morphology closer to what we observe on glass. To
 99 rule out any effect due to changes in the bacterial growth rate, we quantified the division time of
 100 bacteria (Fig. 1C), and the volume occupied by bacterial colonies after a few hours (Fig. 1D and E) on
 101 different substrates: both were found to be unaffected, suggesting that bacteria develop and colo-
 102 nize substrates at the same rate irrespective of rigidity, but that the processes that drive their self-
 103 organization into colonies are modified. In contrast, a change in the morphology of the colonies
 104 could be confirmed by quantifying the characteristic roughness of the bacterial layer, which de-
 105 creases as rigidity increases (Fig. 1E), and the distribution of bacteria with the distance from the
 106 surface, which spreads further for soft hydrogels (Fig. 1F). To control that this is a robust phe-
 107 nomenon driven by substrate elasticity rather than specific chemical interactions, we reproduced
 108 this assay using polyethylene glycol (PEG) hydrogels, which are chemically different from PAA but
 109 can span a similar range of rigidities. We obtained very similar results regarding the phenotype of

110 colonies, which further confirms a role for the mechanical properties of the substrate in bacterial
 111 self-organization (Fig.1-fig. suppl. 2). Finally, because shear flow can orient polarly-attached bacte-
 112 ria, direct motility, disperse quorum-sensing molecules, and generally impact spatial organization
 113 into colonies, we carried out experiments on hydrogels immobilized at the bottom of wells, with-
 114 out any agitation of the above medium. Although long-term observations are rendered difficult in
 115 that case by swimming bacteria, we clearly observed the formation of denser colonies on softer
 116 PAA (Fig.1-fig. suppl. 3), which further demonstrates that substrate stiffness modifies bacterial
 117 behavior after attachment in a wide variety of environments.

118 Since surface motility is known to be important for initial self-organization of PA, we hypothe-
 119 size that it could play a role in the different microcolony shapes that we observe. This link was ex-
 120 plored by carrying out experiments using a mutant deprived of type IV pili (T4P), and thus unable to
 121 twitch on surfaces (mutant PAO1 *pilA::Tn5*, Fig.1-fig. suppl. 4). In these assays, the dependence of
 122 microcolony morphology on substrate rigidity is abolished and bacteria form dense hemispherical
 123 colonies on all PAA substrates. We therefore conclude that T4P-mediated surface motility ("twitch-
 124 ing") plays a key role in the rigidity modulation of microcolony formation by WT PAO1 on soft elastic
 125 substrates.

126 **Substrate elasticity modulates twitching motility**

127 Experimental results - global motility

128 To quantify the coupling between the elasticity of the substrate and the twitching motility of bacte-
 129 ria, we analyzed time-lapse phase contrast images of adhering bacteria in flow cells. These images
 130 allow segmentation of individual bacteria (SI subsection I.A) from the start of the acquisition (with
 131 a few isolated bacteria per field of view) until the transition to out-of-plane growth, after which
 132 individual bacteria cannot be easily separated anymore. From segmented binary images at early
 133 imaging stages (<100 min), we obtain the surface coverage $A(t)$ as the fraction of occupied pixels,
 134 and the cumulative explored area $S(t)$ as the fraction of pixels that has been explored at time t
 135 (Fig. 2A). The evolution of $A(t)$ reflects the exponential growth of initially attached bacteria on the
 136 surface, as well as potential attachment and detachment events during the acquisition. However,
 137 in our experiments initial surface coverage is extremely low, and at early times the number of bac-
 138 teria in the clean flowing medium is negligible so that attachment events are rarely observed. We
 139 can thus consider that

$$\frac{dA}{dt} = (k_{di} - k_{de})A(t). \quad (1)$$

140 The bacterial division rate k_{di} does not depend on the substrate (Fig. 1C), and was measured for
 141 each experiment ($k_{di}^{-1} = 27.8 \pm 1.4$ min). Fig. 2B shows the experimental time evolution of $A(t)$
 142 depending on the gel rigidity, which can indeed be well described by a simple exponential (straight
 143 line in the semi-log presentation with slope $k_{di} - k_{de}$). The slope of $A(t)$ slightly increases with gel
 144 rigidity, suggesting a higher detachment rate k_{de} on softer hydrogels at early acquisition times.

145 Compared to $A(t)$, there is a quantitatively much larger dependence of the cumulative surface
 146 coverage $S(t)$ on the substrate rigidity (Fig. 2B). We propose that this result directly reflects a change
 147 of the global motility V_g of bacteria on the surface. Indeed, neglecting bacterial surface attachment,
 148 the evolution of S can be written as

$$\frac{dS}{dt} = k_{di}A + V_g w_b N = (k_{di} + \frac{V_g}{l_b})A. \quad (2)$$

149 where N denotes the number of bacteria on the surface, and the typical size of a rod-shaped
 150 bacterium is $w_b l_b$ (width \times length), so that the occupied area is $A = N w_b l_b$. Here we have assumed
 151 that bacteria tend to move along their major axis, neglecting reorientations, based on previous
 152 findings about the polar localization of T4P (Cowles and Gitai, 2010; Jin et al., 2011; Kühn et al.,
 153 2021) and our own observations. (Considering that bacteria can move in any direction would lower
 154 velocity values by a factor $\sqrt{\frac{l_b}{w_b}} \approx \sqrt{3}$, and not change significantly the coming discussion.) The

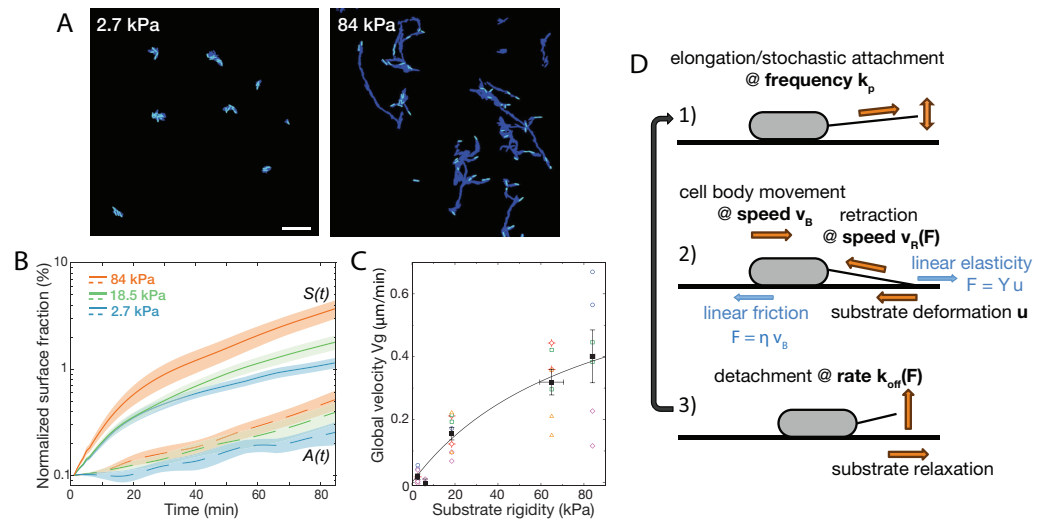


Figure 2. Bacterial surface motility is impaired on soft hydrogels. (A) Surface explored (dark blue) and current surface coverage (cyan) after 100 min on soft and stiff PAA surfaces. Scale bar: 20 μm . (B) Surface coverage $A(t)$ (broken lines) and cumulative explored area $S(t)$ (full lines) for all tested rigidities (the initial surface coverage $\langle A(t = 0 - 10\text{min}) \rangle$ was normalized to 0.1%). Shaded areas are standard errors of the mean (84 kPa: 6 data sets from 3 independent experiments, 18.5 kPa: 10 data sets from 5 independent experiments, 2.7 kPa: 8 data sets from 4 independent experiments). (C) Global bacterial motility V_g averaged over the first 100 min, inferred from the difference between $A(t)$ and $S(t)$ (16 different surfaces, 6 independent experiments). The black line is the fit with the kinetic model using equation A11, with values $V_{\text{max}} = 0.77 \pm 0.35 \mu\text{m} \cdot \text{min}^{-1}$ and $E_0 = 84 \pm 68 \text{ kPa}$. (D) Ingredients of the minimal 1D model for bacterial T4P-powered displacement.

155 average bacterial size was measured in each experiment ($l_b = 2.8 \pm 0.13 \mu\text{m}$, $w_b = 0.8 \pm 0.13 \mu\text{m}$).
 156 For each monitored position, we determined dS/dt and $A(t)$ experimentally. The global bacterial
 157 velocity V_g was then estimated using Eq. 2, by averaging over the first 100 experimental time points.

158 During the first 100 minutes under flow, V_g exhibits a clear dependence on substrate elastic-
 159 ity (Fig. 2C). Motility values are close to zero on very soft substrates (3-6 kPa), and progressively
 160 increase to reach $\sim 0.5 \pm 0.25 \mu\text{m}/\text{min}$ on the stiffest hydrogels tested in this study (84 kPa). We
 161 wondered whether this dependence of surface motility on substrate elasticity could result from
 162 intracellular modifications in response to bacterial surface-sensing. In *P. aeruginosa*, two main
 163 surface-sensing systems have been unveiled so far: the Pil-Chp system that involves T4P retraction-
 164 mediated force sensing *Webster et al. (2022)*, and the Wsp system believed to be activated by cell
 165 envelop stress *ONeal et al. (2022)*; both systems have been shown to activate biofilm formation
 166 pathways following bacterial adhesion *Chang (2018)*. Sessility and matrix production are promoted
 167 by increasing intracellular c-di-GMP levels, which production is catalyzed by diguanylate cyclases
 168 (DGCs). We carried out experiments with *wspR* and *sadC* mutants, two DGCs known to be involved
 169 in the surface-sensing response. Although impaired in c-di-GMP regulation, both mutants still ex-
 170 hibited a stiffness-dependent twitching motility (Fig.2-fig. suppl. 1). Even though other DGCs might
 171 be involved, these initial results suggests that our observations at early timescales could be mainly
 172 governed by the mechanical interaction of bacteria with their substrate, with gene regulation play-
 173 ing a secondary role. This rationale motivates the simple kinetic modelling presented next.

174 Minimal kinetic modelling

175 Because a difference in twitching velocity is observed almost immediately upon attachment of
 176 bacteria onto the surface, a simple hypothesis could be that a modulation of the twitching efficiency
 177 arises through mechanical factors - the interplay between the T4P extension/retraction mechanism
 178 and the linear elasticity of the substrate - without the need for mechanotransduction mechanisms.
 179 To test this minimal hypothesis, we have developed a kinetic model, schematically described on

180 figure 2D.

181 Briefly (more details can be found in appendix 1), we consider a bacterium adhering onto an
 182 elastic substrate with a single effective pilus. The pilus is modelled as a rigid inextensible filament
 183 (Beaussart *et al.*, 2014) and attaches to the substrate via its extremity with a typical adhesion size λ .
 184 This simple choice is motivated by microscopic observations of pilus straightening over its whole
 185 length during retraction Talà *et al.* (2019) and an estimation of the pilus attachment spot size of
 186 ≈ 1 nm from traction force microscopy measurements Koch *et al.* (2022). Note, that multiple at-
 187 tachments of pili over extended regions to the substrate have also been suggested Lu *et al.* (2015).
 188 However, in our simple approach we do not consider this possibility.

189 The cell actively retracts its pilus until it detaches from the substrate with the force dependent ve-
 190 locity $v_R(F) = v^0(1 - \frac{F}{F_R})$ (Marathe *et al.*, 2014), where F denotes the tensile load on the pilus, F_R
 191 the retraction stall force and v^0 the retraction speed at zero load. Assuming linear elasticity, the
 192 tensile load F is related to the substrate displacement u at the pilus adhesion patch by $F = Yu$,
 193 where $Y \sim E\lambda$ and E is the Young's modulus of the substrate. Since the typical size of the bacterial
 194 body l_b is much larger than λ , we neglect the deformation of the substrate induced by the bacterial
 195 body. Instead we assume that the pilus tension leads to a forward sliding of the bacterial body with
 196 a linear force-velocity relationship $v_B(F) = v^0 \frac{F}{F_B}$ (see SI subsection II.B and (Sens, 2013)), reducing
 197 the substrate deformation and the load in the pilus. Here, the ratio $\eta = \frac{F_B}{v_0}$ denotes the mobility
 198 constant of the cell on the substrate. With this model, the evolution of the pilus tension F is thus
 199 given by

$$\frac{dF}{dt} = Y \frac{du}{dt} = v_R(F) - v_B(F) \quad (3)$$

200 which is solved by

$$F(t) = F_0 \left(1 - e^{-\frac{Yv^0}{F_0}t} \right) \quad (4)$$

201 with the naturally arising force scale

$$F_0 = \frac{F_B F_R}{F_R + F_B}. \quad (5)$$

202 From $\frac{dx_B}{dt} = v_B(F)$ we obtain the bacterial sliding distance during the pilus retraction

$$x_B(t) = \frac{F_0}{F_B} \left[v^0 t + \frac{F_0}{Y} \left(e^{-\frac{Yv^0}{F_0}t} - 1 \right) \right]. \quad (6)$$

203 While retracting the pilus will detach with a rate constant k_{off} from the substrate. Assuming a force-
 204 independent off-rate constant $k_{\text{off}} = k_{\text{off}}^0$ (and hence a mean pilus adhesion time $(k_{\text{off}}^0)^{-1}$) and a pilus
 205 retraction frequency k_p , we obtain an effective bacteria velocity:

$$v_{\text{eff}} = k_p \langle x_B \rangle = k_p k_{\text{off}}^0 \int_0^{\infty} x_B(t) e^{-k_{\text{off}}^0 t} dt = V_{\text{max}} \frac{E}{E + E_0}. \quad (7)$$

206 Here, $\langle x_B \rangle$ denotes the mean bacterial sliding distance per pilus retraction event and V_{max} denotes
 207 the maximum effective speed a bacterium can reach on a given substrate at infinite rigidity. It is
 208 given by

$$V_{\text{max}} = v^0 \frac{k_p}{k_{\text{off}}^0} \frac{F_R}{F_B + F_R}. \quad (8)$$

209 E_0 denotes the rigidity at half-maximal speed and is given by

$$E_0 = \frac{F_B F_R k_{\text{off}}^0}{(F_B + F_R) v^0 \lambda}. \quad (9)$$

210 Fitting (A11) against experimentally measured effective bacterial velocities V_g provides a quantita-
 211 tive description of the data for $V_{\text{max}} = 0.77 \pm 0.35 \mu\text{m} \cdot \text{min}^{-1}$ and $E_0 = 84 \pm 68$ kPa. The error estimates
 212 for V_{max} and E_0 were calculated directly from the co-variance matrix of the fit function and the
 213 variance of residuals (chi-squared sum divided by the number of degrees of freedom) and are re-
 214 flective of the wide scattering of measured velocities between different experiments. Conversely,

215 we can estimate V_{\max} and E_0 from values of the parameters used in the model: assuming a typical
216 pilus retraction speed $v^0 = 1 \mu\text{m}\cdot\text{s}^{-1}$ (Marathe et al., 2014), a stall force of the order $F_R = 100 \text{ pN}$
217 (Marathe et al., 2014; Koch et al., 2022), a pilus off-rate constant $k_{\text{off}}^0 = 1 \text{ s}^{-1}$ (Talà et al., 2019), a
218 contact size of $\lambda = 1 \text{ nm}$ (Koch et al., 2021), a high friction surface with $F_B = 1 \text{ nN}$ and a typical pilus
219 retraction frequency¹ of $k_p = 0.2 \text{ s}^{-1}$ we obtain $V_{\max} \sim 1 \mu\text{m}\cdot\text{min}^{-1}$ and a substrate rigidity at half
220 maximum speed of $E_0 = 100 \text{ kPa}$, which are within 30% of the fitted values.

221 In addition, our model [Eq. (8)] shows that two separate effects translate a (fast) load-free micro-
222 scopic pilus retraction speed v^0 into a (slow) macroscopic bacterial speed V_{\max} . First, the bacterium
223 only translocate during a fraction of the pilus cycle of extension and retraction $\frac{k_p}{k_{\text{off}}}$ over the sub-
224 strate. Second, the pilus retraction speed slows down in a load dependent manner $F_R/(F_B + F_R)$.
225 Both effects together reduce the local speed by an order of magnitude from $\mu\text{m}\cdot\text{s}^{-1}$ to $\mu\text{m}\cdot\text{min}^{-1}$.

226 Together this demonstrates that our experimental results on bacterial effective motility on elas-
227 tic substrates can be interpreted as the result of a simple interplay between the pilus retraction
228 mechanism, the deformation of the elastic substrate, and the friction of the bacterial body on this
229 substrate.

230 Analysis of individual trajectories

231 The simple approach presented Fig. 2 yields a population-averaged value of the bacterial velocity
232 V_g . Yet, bacterial populations can be heterogeneous, and moreover the model we have used Eq. (2)
233 to determine V_g relies on a number of strong assumptions, such as neglecting detachment and re-
234 attachment events. To go further in dissecting bacterial motility on PAA substrates, we developed a
235 segmentation and tracking protocol in order to obtain the individual tracks of all the bacterial cells
236 visible over the course of the acquisition (Fig. 3A, Video 2 and Methods and Materials for details).
237 This thorough approach allows us to measure the velocity associated with each 1-min displacement
238 step.

239 Can a characteristic twitching velocity be defined for all bacteria? or do phenotypically distinct
240 populations of slow and fast bacteria cohabit on the surface? To answer these questions, we la-
241 beled each track, defined as the displacement of a bacterium between two successive division
242 events (Fig. 3A). We expected track duration to be similar to the characteristic division time shown
243 on Fig. 1C. However, we obtained a bimodal distribution, with two peaks centered at times unaf-
244 fected by the substrate rigidity: one peak indeed centered on the division time ($\sim 27 \text{ min}$), and a
245 second one that corresponds to bacteria spending 5 to 10 min on the surface before detaching
246 (Fig.3-fig. suppl. 1A). The velocity distribution corresponding to each population is similar (Fig.3-fig.
247 suppl. 1B). This observation is consistent with a phenotypical difference between daughter cells,
248 in agreement with the results of (Laventie et al., 2018) Indeed, the duration of the track before
249 detachment tends to be shorter on soft substrates, but the fraction of bacteria that detach from
250 the substrate ($35 \pm 2 \%$) is independent of the substrate rigidity. We thus assume that at early ex-
251 perimental timepoints, after moving in sync with the first daughter cell, the second one sometimes
252 detaches from the substrate (about 70% of the time). This feature might change at later timepoints
253 - bacterial tracking was interrupted at the onset of 3D spatial organization ($\sim 100 \text{ min}$ on the softest
254 hydrogels, see next section for a full description).

255 Considering only adhering offsprings, for which full tracks were recorded, we normalized tracks
256 with respect to their initial position, yielding Fig.3A. These homogeneous radial distributions con-
257 firm that shear does not influence bacterial orientation in our experiments. As expected, track
258 extension becomes larger as substrate rigidity increases. The distribution of the mean velocity of
259 tracks does not allow us to distinguish different bacterial sub-populations: it reaches higher values
260 on stiffer hydrogels, but it is broad, continuous with an exponential decay (reflecting the diversity
261 of behaviours expected in a population of cells) (Fig. 3B). In addition, for each track the standard
262 deviation of this mean velocity is comparable and proportional to its mean (Fig.3-fig. suppl. 2),

¹Here we assume that one single effective pilus is active during a retraction event. Using a typical pilus length of $5 \mu\text{m}$ with retraction speed of $v_0 = 1 \mu\text{m}\cdot\text{s}^{-1}$ we obtain a duration of 5 s per retraction and a retraction frequency of 0.2 s^{-1}

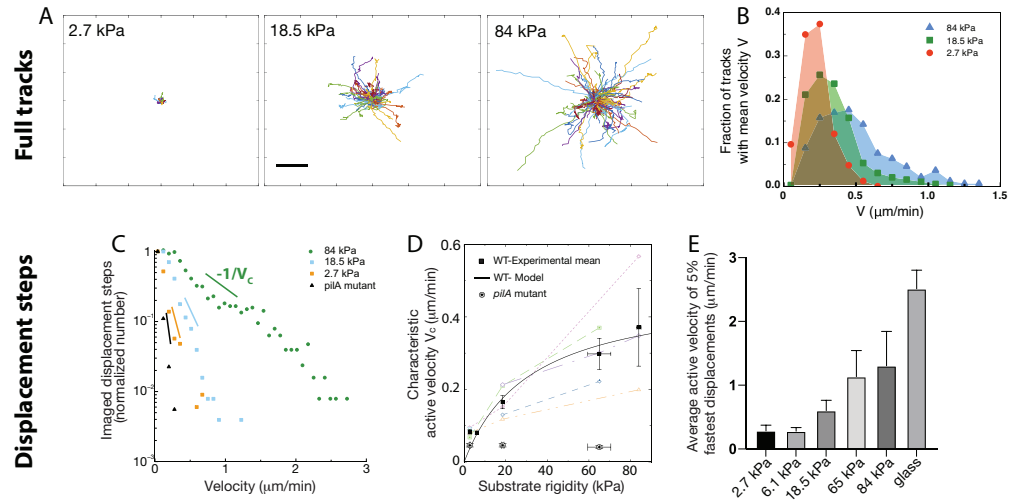


Figure 3. Twisting motility depends on substrate rigidity and is highly distributed in the bacterial population. Analysis of full tracks (top row) and 1-min displacement steps (bottom row). (A) Individual bacterial tracks on soft (2.7 kPa), intermediate (18.5 kPa) and stiff (84 kPa) PAA during the first 3 hours after bacterial inoculation (total number of tracks is respectively 60, 123 and 175). Scale bar: 10 μm (B) Mean track velocity distribution for different values of the substrate rigidity. Only full tracks were considered (corresponding to the right peak in fig. suppl. 1). 84 kPa: 330 tracks from 2 independent experiments, 18.5 kPa: 394 tracks from 3 independent experiments, 2.7 kPa: 83 tracks from 2 independent experiments. (C) Normalized velocity distributions for the whole bacterial population on different PAA surfaces. The exponential decrease yields a characteristic active velocity V_C on each substrate. Displacement steps were measured every minute for 100 minutes, and two positions were acquired on each rigidity. The average of T4P-defective mutant on all surfaces is shown as a reference. (D) Characteristic active velocity values V_C obtained by fitting velocity distributions (6 independent experiments, 16 different surfaces). Values measured on different surfaces in a single experiment (same channel) are shown with the same symbols and connected. Black squares(circled stars) are mean values obtained for the WT(*pilA* mutant), and error bars show the SEM. The black line is the fit of WT values with the kinetic model-derived equation A11, with $V_{\text{max}} = 0.48 \pm 0.12 \mu\text{m} \cdot \text{min}^{-1}$ and $E_0 = 32 \pm 30 \text{ kPa}$. (E) Average velocity values of the top 5% fastest displacement steps for different substrates. Error bars are standard errors.

263 suggesting a stochastic distribution of twitching steps within a given trajectory.

264 Focusing next on 1-min displacement steps, and pooling all monitored events during the first
265 100 min of experiments (which provides more data than only analysing full tracks within the same
266 time window), we obtained the typical velocity distributions shown on figure 3C. These distributions
267 further confirm that bacterial displacements are very heterogeneous, and present an exponentially
268 decreasing tail which fitting yields a characteristic velocity V_C for the bacterial population on a given
269 substrate, i.e.:

$$N(V > V_0) = N_0 \exp\left(-\frac{V - V_0}{V_C}\right), \quad (10)$$

270 ($V_0 = 0.08 \mu\text{m}/\text{min}$ denotes a visual cutoff for low velocities).

271 To rationalize the meaning of V_C , we reasoned that displacement steps are the sum of a passive
272 velocity due to bacterial elongation, local reorganisations and experimental noise, and an active ve-
273 locity powered by T4P. The velocity distribution obtained using a *pilA* mutant is purely exponential,
274 and was used to determine the characteristic passive motility, which does not significantly depend
275 on substrate rigidity ($V_C(\text{pilA}) = V_{C,p} = 0.044 \mu\text{m}/\text{min}$, see Fig. 3D). In the case of motile strains, as-
276 suming that active and passive displacements are incoherent, our numerical calculations (Fig. 3-fig.
277 suppl. 3) show that in the limit $V_C > V_{C,p}$, the fitted characteristic velocity V_C obtained as described
278 above reflects the active twitching motility of the population, and is not significantly affected by
279 passive movements. A detailed justification for our analysis of the probability distributions of dis-
280 placement steps is given in the Methods section.

281 This analysis, which does not rely on any strong assumption, yields active velocity values for the
282 WT strain (Fig. 3D) in very good qualitative agreement with the global velocity analysis described
283 earlier (V_g , Fig. 2C, and Fig. 3-fig. suppl. 4). Again, our kinetic model describes the data quantita-
284 tively with values very close to the ones fitted and calculated in the previous subsection ($V_{\text{max}} =$
285 $0.48 \pm 0.12 \mu\text{m} \cdot \text{min}^{-1}$ and $E_0 = 32 \pm 30 \text{ kPa}$). The large error bars on fitting parameters reflect the
286 dispersion of experimental measurements, despite our efforts to reproduce identical experiments.
287 However, velocity values measured in a given experiment always exhibit a similar dependence on
288 substrate rigidity, i.e. a clear increase of motility as rigidity increases. In addition, we characterized
289 the velocity of the 5 % fastest bacterial displacement steps (Fig. 3E) on each type of substrate. This
290 analysis confirms the dependence of twitching velocity on substrate rigidity, but also yields higher
291 velocity values, in good quantitative agreement with those reported in the literature using other
292 experimental approaches (Talà *et al.*, 2019), which might be biased towards more active bacte-
293 ria. Finally, this approach was used to quantify bacterial motility in experiments on PEG hydrogels
294 (shown Fig. 1 - fig.supp.), which confirms the very similar bacterial behaviour on the two kinds of
295 substrates we have used (Fig. 3-fig. suppl. 5).

296 **Rigidity-modulated bacterial motility governs the spatial characteristics of early** 297 **surface colonization**

298 In-plane to 3D transition of emerging colonies

299 To understand the way rigidity-modulated bacterial motility impacts the process of microcolony
300 formation, we studied in details the way colonies transition to out-of-plane growth. Several ex-
301 perimental and theoretical approaches have been developed in the past to decipher this process:
302 for confined colonies, the switch from planar to 3D growth takes place when it becomes energeti-
303 cally too costly to push neighboring cells outwards. In that case, the adhesion forces between the
304 bacteria and their underlying substrate play a key role: strongly adhering bacteria transition to
305 3D colonies earlier in their development (Duvernoy *et al.*, 2018; Grant *et al.*, 2014). In our exper-
306 iments, there is no strong vertical or lateral confinement: bacteria can move on the substrate or
307 away from it, so that cells stemming from a given progenitor do not necessarily stay in contact with
308 each other. However, the twitching velocity determines how much cells, on average, move away
309 from one another between two successive division events, thereby creating space to accommodate
310 new offsprings on the surface.

311 To investigate the possible link between twitching motility and 2D to 3D transition of growing
312 microcolonies, we sought to determine N_c , the number of adhered cells in a progeny (i.e. stemming
313 from successive divisions of a given bacterium) when the 2D to 3D transition takes place, as a
314 function of the twitching velocity. For softer substrates, all bacteria can be imaged, and N_c is directly
315 measured; we also determined the average number of colonies per unit area. On stiffer substrates,
316 it is impossible to track all bacteria stemming from a mother cell, since they are very motile and
317 sometimes move out of the field of view. We assume that bacteria from other progenies are equally
318 likely to move inside the field of view, so that measuring the number of bacteria on the image at
319 t_c (the time at which transition to 3D is first observed), divided by the average microcolony density
320 determined on softer substrates earlier gives a good approximation of N_c . Fig. 4A shows N_c as a
321 function of the center-of-mass characteristic velocity V_C determined above (Fig. 3D), on different
322 substrates and for 9 different experiments. N_c consistently increases with the twitching velocity,
323 indicating a strong correlation between the twitching efficiency and the shape of early colonies and
324 shedding light on our initial observations of variations in microcolony morphology as a function of
325 the substrate rigidity (Fig. 1B, D-F).

326 To decipher the link between N_c and V_C , we have built a simple kinetic model with a single
327 unknown parameter (see appendix 2 for details). Briefly, we assume that the 2D to 3D transition
328 takes place when the area occupied by bacteria reaches a fraction of the equivalent "microcolony
329 size", defined as the characteristic area explored by bacteria in a progeny. Assuming that bacteria
330 explore the surface through a random walk with persistence (*Marathe et al., 2014*), the charac-
331 teristic area accessible to bacteria in a microcolony over time can be written as $a(t) = a_0(1 + \alpha V_C t)$
332 where a_0 is the area of one bacterium and α is a parameter related to the properties of the random
333 walk. Our experimental data show that not only the velocity, but also the contour length of the
334 trajectories of bacteria increases with the rigidity since the duration of these trajectories is mostly
335 constant (Fig. 4B and Fig. 3-fig. suppl. 1). Area $a(t)$ is related, but not equal, to the area over which
336 the microcolony spreads. Indeed, bacteria are not evenly distributed within the microcolony area,
337 and we observe strong local density fluctuations. If we now consider an exponential growth of the
338 number of bacteria on the surface due to the balance of cell division and detachment, it follows
339 that the increase in the number of cells, and hence the area required to accommodate these cells
340 on the surface, grows faster than the accessible area, driving a transition to 3D growth. Expressing
341 the number of cells N_c in the microcolony at the time when this transition stochastically occurs
342 leads to the following dependence as a function of V_C :

$$N_c = 1 + \gamma V_C \log(N_c) \quad (11)$$

343 γ is an unknown parameter related to the properties of the random walk and the growth rate of
344 bacteria on the surface that can be measured for each experiment. On figure 4A, we have plotted
345 the corresponding curve using the average of experimental values for γ (solid line) \pm their standard
346 deviation (dotted lines). We observe an excellent agreement between this simple kinetic model and
347 our experimental data over a wide range of velocities, including the T4P deficient mutant and the
348 WT strain adhering on glass. This hints that elasticity is a key factor shaping the organization of early
349 colonies on elastic substrates, and that it is the main determinant of the colony shapes observed
350 in our experiments on chemically identical substrates with varying rigidities (rather than energy
351 minimization whereby bacteria would either favour adhesion to other cells or to the substrate
352 depending on its rigidity).

353 Surface decoration by extracellular matrix

354 One consequence of the modulation of twitching efficiency by the substrate elasticity could be a
355 variation in matrix distribution on the surface. Indeed, *P. aeruginosa* can secrete an extracellular
356 matrix mostly composed of exopolysaccharides (EPS), which was shown to result in the deposi-
357 tion of "trails" by twitching bacteria on glass substrates. By mediating the attachment of the cell
358 body to the underlying substrate such deposits are inferred to facilitate further colonisation by

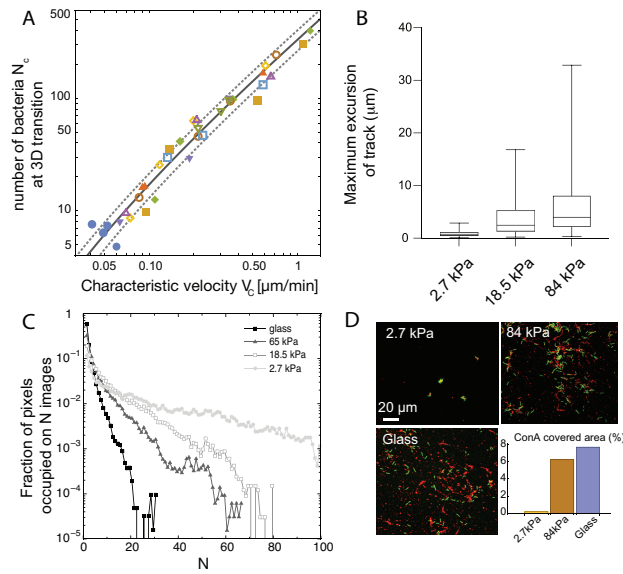


Figure 4. Spatial structuring of surface colonization is impacted by substrate rigidity through twitching velocity. (A), size of microcolony (in number of bacteria N_c) at the 2D to 3D transition as a function of the center-of-mass characteristic velocity V_c defined in Fig. 3A. Markers are experimental data from 9 different experiments, each with different substrates including glass (hence leading to higher values than in Fig. 3B). Blue dots are data obtained with the pili-deficient mutant $\text{pilA}::\text{Tn5}$. Lines, kinetic model for $\langle \gamma \rangle$ (solid line) \pm its standard deviation (dotted lines). (B) Distribution of track lengths of full trajectories as a function of the substrate rigidity. (C) Distribution of occupation occurrence on each image pixel as a function of rigidity, showing a much more heterogeneous occupancy on soft substrates. (D), ConA staining (red) of EPS deposition during cell (green) exploration of the surface.

359 bacteria and to impact microcolony formation (Liu et al., 2007; Zhao et al., 2013). To investigate
 360 matrix deposition on hydrogel substrates, we introduced a fluorescent dye (lectin concanavalin A,
 361 see Methods and Materials) in the nutrient medium infused in our device. The main component
 362 of PAO1 matrix, psl (Jackson et al., 2004), is rich in mannose, that conA specifically binds (Ma et al.,
 363 2007).

364 For high stiffness substrates where bacteria explore the surface efficiently, this staining confirms
 365 that trails of matrix decorate a significant fraction of the surface; on the contrary, nearly immo-
 366 bile bacteria on soft substrates accumulate matrix locally, leaving most of the surface unmodified
 367 (Fig.4C and D). This difference in matrix distribution is maintained at a later stage of surface colo-
 368 nization (Fig.4-fig. suppl. 1). While on rigid hydrogels, most of the surface is covered by bacteria-
 369 secreted matrix, lectin staining on soft hydrogels is only present on compact colonies separated
 370 by regions completely devoid of EPS. While proper quantification of the total amount of matrix
 371 produced in each case is difficult (staining efficiency might be impacted by lectin diffusion inside
 372 dense colonies), our results confirm that substrate rigidity impacts bacterial propensity to modify
 373 hydrogel substrates via matrix deposits.

374 Substrate rigidity affects bacterial mixing

375 Real-life biofilms generally comprise several species: pathogens can compete or help each other
 376 (DeLeon et al., 2014; Orazi et al., 2017), and commensal strains protect organisms from detrimen-
 377 tal ones (Aoudia et al., 2016). To further investigate how modulation of surface colonization with
 378 rigidity impacts the structure of forming biofilms, we studied the model co-colonization of hydro-
 379 gels by two PAO1 strains constitutively expressing two different fluorescent proteins. Beside their
 380 fluorescence, the two strains exhibit identical properties (motility, division rate, etc.), similar to
 381 that of WT PAO1. Through fluorescent confocal imaging, the strains were spectrally separated to

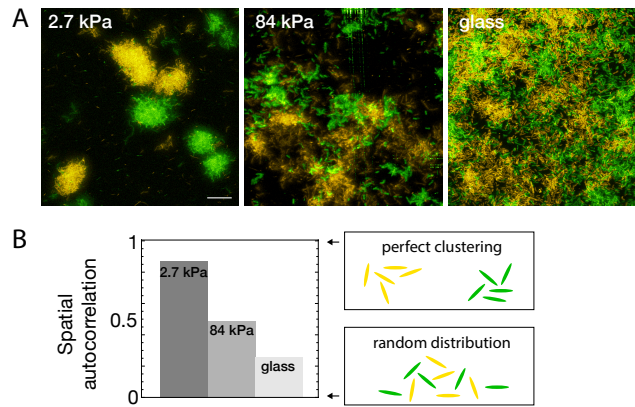


Figure 5. Bacterial spatial distribution is impacted by substrate rigidity. (A) Images of surfaces seeded with a 1:1 mixture of constitutively fluorescent bacteria expressing GFP or YFP show mostly monoclonal colonies on soft hydrogels, and mixed bacteria on rigid substrates (3D-rendering obtained by stacking images). Scale bar, 20 μm . (B) Spatial correlations quantified via Moran's I index.

382 study their spatial distribution at different stages of surface colonization. As expected, rigidity-
 383 modulated motility impacts the co-colonization of the hydrogels from early stages (Fig.5-fig. suppl.
 384 1): on rigid substrates, high motility promotes mixing of the offsprings of different cells, resulting in
 385 a spatial distribution of the two strains close to random (a residual correlation between the colour
 386 of neighbouring cells is always found due to the presence of cells that have just divided). Con-
 387 versely, nearly immobile cells on soft substrates exhibit strong correlations between neighbouring
 388 cells, which mostly arise from a single progenitor cell. This striking difference in strain mixing dur-
 389 ing surface co-colonization is maintained at later stages of biofilm formation: on soft substrates,
 390 quasi-monoclonal colonies with complete spatial segregation are observed, while biofilms forming
 391 on rigid surfaces exhibit a close-to-random distribution of the two strains at the 10- μm scale (Fig.
 392 5A). To quantify this effect, we have used Moran's I index, a statistical tool designed to quantify
 393 the spatial clustering of species. It provides a measure of the local spatial correlations and takes
 394 values ranging from 1 (perfectly correlated values) to -1 (perfectly anti-correlated values), with 0
 395 corresponding to a spatially random distribution of the variable (see Methods and Materials for
 396 details). The resulting quantitative analysis (Fig. 5B) confirms the decisive impact of rigidity on
 397 the structure of mixed biofilms, with potentially far-reaching consequences on the interactions of
 398 different strains in multi-species biofilms.

399 Surface rigidity impacts gene expression

400 Cell-cell communication, either via exported molecules or by direct contact is crucial during biofilm
 401 development (*Shrout et al., 2011*). Modifications of bacterial distribution as described above could
 402 thus likely impact gene regulation in surface-attached bacteria. To start addressing this complex
 403 question, we focused on the expression level of cyclic-di-GMP (c-di-GMP), a second messenger that
 404 controls the motile-to-sessile transition in *P. aeruginosa* (*Rodesney et al., 2017*). We used a post-
 405 transcriptional fluorescent reporter build on the promoter of the gene *cdrA*, which encodes an
 406 exported protein involved in matrix cohesion, upregulated during biofilm formation by PAO1 (*Re-
 407 ichhardt et al., 2018*). The PcdrA-gfp intracellular reporter provides a measure of the integrated
 408 production of CdrA with a ~ 40 min delay between expression of the gene and fluorescence detec-
 409 tion (*Rybtke et al., 2012*). Fig. 6 shows how *crdA* expression is modulated by rigidity on 4 substrates
 410 included in the same microfluidic device. For this reporter, the degradation rate of gfp occurs over
 411 several hours, and its dilution due to growth and division of bacteria occurs at the same rate on
 412 all surfaces (see Fig. 1C). The increase rate of the fluorescence signal is thus a direct proxy to the
 413 expression rate of gene *cdrA*, and thus to the changes in c-di-GMP level.

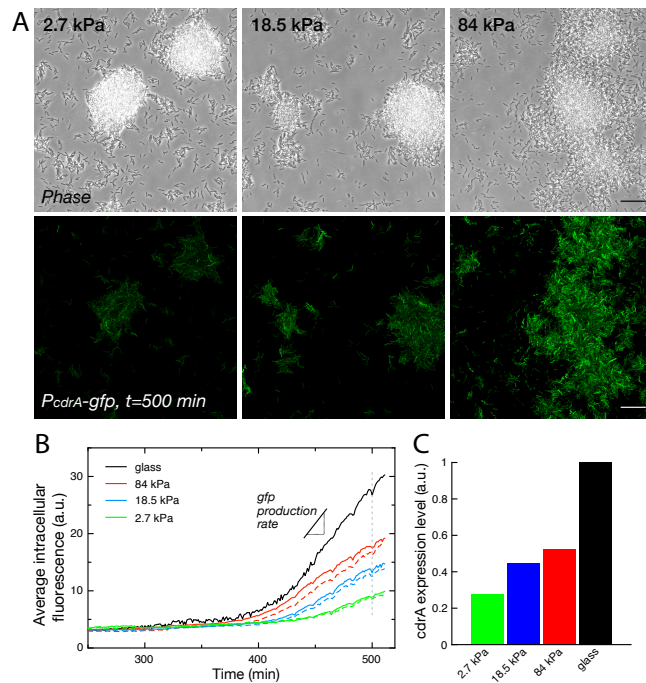


Figure 6. Substrate rigidity influences gene expression levels (A) Colonies grown from a modified PAO1 strain bearing the plasmidic $P_{cdrA} - gfp$ reporter imaged in phase contrast (top) and fluorescence (bottom), after 500 min under flow. Scale bars, 20 μm . (B) Average intracellular gfp fluorescence as a function of time, on different PAA surfaces and on glass. Broken lines are duplicate positions on a given surface. (C) Average $cdrA$ expression level, obtained from a linear fit of (B).

414 During a first phase of surface colonization, fluorescence remains low on all surfaces. The sig-
 415 nal subsequently starts increasing linearly, roughly at the same time for all surfaces (within the
 416 uncertainty of fluorescence quantification, i.e. ≈ 10 minutes). This second phase ends with the on-
 417 set of a plateau, again around the same time for all surfaces, at the end of the exponential growth
 418 of bacteria adhered on the surface, possibly as a result of oxygen depletion in the flowing medium
 419 that would be sensed simultaneously on all surfaces (Fig. 6-fig. suppl. 1). This linear increase in flu-
 420 orescence directly translates into a constant production rate of CdrA that can be compared for the
 421 4 surfaces (Fig. 6C): our analysis shows a marked increase in CdrA expression with the substrate
 422 rigidity.

423 Discussion

424 In this study, we have designed an experimental approach to investigate early microcolony forma-
 425 tion by *P. aeruginosa* on hydrogels with different elastic moduli, under constant flow rate. By con-
 426 tinuously imaging surface-attached bacteria *in situ*, we show that substrate rigidity influences the
 427 twitching motility of individual bacteria, therefore strongly impacting the process of microcolony
 428 formation. Through two different analyses of the surface motility of the bacterial population, ei-
 429 ther via the global evolution of the explored area or via the tracking of individual cells, we find that
 430 the characteristic twitching velocity increases with substrate stiffness (from 0.02 to 0.4 $\mu\text{m}/\text{min}$
 431 when rigidity goes from ~ 3 to 80 kPa).

432 The encounter between bacteria and a substrate generates mechanical stress. Deciphering surface-
 433 sensing, i.e. understanding how the mechanical feedback resulting from this interaction translates
 434 into chemical signals that will in turn tune bacterial behavior has been the focus of a lot of recent
 435 research. It is now clear, for instance, that T4P contraction acts as a force sensor that transmits
 436 signals to the bacterium at the single-cell level (Webster *et al.*, 2022), and triggers a response that
 437 involves an increase in c-di-GMP level (Armbruster *et al.*, 2019). Furthermore, recent results sug-

438 gest that pili can differentiate substrate rigidity, yielding a maximum response for stiffness values
439 ~ 300 kPa *Koch et al. (2022)*.

440 However, in our experiments a difference in bacterial motility can be observed almost immediately
441 upon surface adhesion to soft or rigid PAA, and this behavior is not modified in mutants impaired
442 in c-di-GMP regulation (*wspR* or *sadC*). We thus propose a physical model to account for the mod-
443 ulation of the twitching motility. This 1D model is based on a force balance between (i) a pilus
444 that extends, attaches and retracts with a defined frequency; (ii) the deformation of the underlying
445 substrate at the pilus tip upon retraction; and (iii) the friction force due to adhesion of the bacte-
446 rial body when it is dragged across the surface at the other end of the pilus. In this balance, the
447 detachment rate of the pilus tip from the substrate is a key parameter in the resulting bacterial
448 velocity. We have assumed a force-independent off-rate constant for the pilus. In a more complex
449 scenario, the contact between the pilus and substrate may act as a slip bond or a catch bond. For
450 completeness we show some numerical results for slip and catch bond behavior in the SI (section
451 I.D), which do not increase however the quality of fit between experimental and theoretical velocity
452 data. In addition, although we have explored the possibility that substrate rigidity, which is directly
453 correlated to the mesh size of the hydrogel network, could impact the frequency of attachment of
454 T4P, this was not necessary to efficiently account for the variation in motility we observe, which we
455 instead solely attribute to the elastic deformation of the substrate.

456 Strikingly, our minimal mechanistic model thus suggests that a variety of observed phenomena
457 (3D structure of colonies; EPS deposition on the surface; strain mixing during co-colonization) can
458 all derive from a modulation of the efficiency of pili activity by the deformability of soft substrates.
459 This purely mechanical model may be of particular importance for surface colonization, since the
460 adaptation of bacterial behaviour to the environment can thus be instantaneous - possibly a key
461 to PA ability to efficiently colonize extremely different microenvironments.

462 While this model is sufficient to account for our observations (twitching velocity, microcolony for-
463 mation), it certainly does not rule out a regulatory response of the bacteria, which probably takes
464 place in parallel. Such a response can happen on two levels: at the single cell level, mechanotrans-
465 duction processes mediated for instance by adhesion and retraction of T4P can influence gene
466 expression at short timescales ($\%1$ hour) *Armbruster et al. (2019)*; *Song et al. (2018b)*. At longer
467 timescales, in developing microcolonies, cell-cell interactions could in turn modulate the bacterial
468 transcriptome, which depends on microcolony characteristics (e.g. shape, cell density, matrix con-
469 tent) *Livingston et al. (2022)*. Our attempt at quantifying c-di-GMP expression using a fluorescent
470 intracellular reporter does evidence a difference in bacterial regulatory response depending on
471 substrate stiffness. While the level of expression of the gene is clearly impacted by the substrate
472 rigidity, differences in expression level are detected only 6-7 hours after the onset of surface col-
473 onization, with a first phase characterized by low c-di-GMP level on all surfaces. This timeframe
474 suggests that the difference in gene expression that we observe is probably not due to a direct
475 sensing of the substrate rigidity by individual bacteria, but rather a consequence of their organiza-
476 tion into more or less dense colonies. Of note, when the increase in c-di-GMP takes place bacteria
477 have stopped twitching and immobilized into colonies. We do not observe the early increase in
478 c-di-GMP described in the literature, possibly because we initially only track a very small number
479 of bacteria on the surface, and the expression signal is stochastic. Further investigating c-di-GMP
480 expression in WT and mutant strains upon adhesion to mechanically different substrates could
481 help reveal which pathways are differently activated on soft substrates.

482 Interestingly, our results show that microcolony phenotype may not be indicative of a specific c-
483 di-GMP regulation. The dense colonies observed on soft hydrogels correspond to lower c-di-GMP
484 levels than the flat bacteria carpets that grow on rigid substrates, a somehow counter-intuitive
485 result given the paradigm that c-di-GMP production upregulates biofilm-inducing genes, in partic-
486 ular matrix production, while downregulating motility. Here, we describe a case when motility is
487 rendered impossible by the micromechanical properties of the environment rather than by the
488 absence of functional pili, thus resulting in the rapid formation of compact colonies on soft sub-

489 strates. Further exploring the density and the exact composition of the extracellular matrix in
490 these colonies would be interesting since this parameter could influence the subsequent fate of
491 bacteria on the surface. EPS distribution, composition and concentration may also be significant
492 for the recruitment of new cells on the surface: indeed, previously deposited matrix is thought to
493 strengthen adhesion of *P.aeruginosa* bacteria (Zhao *et al.*, 2013), and could also possibly mediate
494 adhesion of other microorganisms.

495 In a wider context, the process we observe could also be envisioned as a strategy to optimize bacte-
496 rial colonization of mechanically heterogenous environments by ensuring accumulation of bacteria
497 into dense colonies located in the softer regions of their environment, e.g. over cellular tissues. Re-
498 cently, Cont *et al.* have shown that dense colonies were able to deform soft substrates and exert
499 forces that could disrupt an epithelium layer (Cont *et al.*, 2020): rigidity-modulated twitching could
500 thus provide *Pseudomonas aeruginosa* with a convenient means of targeting soft tissues for coop-
501 erative disruption and subsequent invasion.

502 The phenotypic differences that we report for colonies are likely to impact subsequent interactions
503 of bacteria with their environment: response to changes in nutrient or oxygen availability, and
504 chemical signals in general which will not efficiently penetrate inside dense colonies. This could in
505 particular influence susceptibility to antibiotics, as confirmed by very recent work Cont *et al.* (2023).
506 This is all the more relevant that PA can invade many different environments, and might have to
507 be treated differently when it settles in the lungs of cystic fibrosis patients, or on the surface of
508 rigid implants.

509 Finally, our data show that rigidity-modulated twitching has a striking impact on the mixing of
510 different strains upon surface colonization. Understanding the mechanisms governing the forma-
511 tion of mixed-species communities is one of the key challenges of current biofilm research. Since
512 the motility modulation mechanism described here is quite general and should be marginally af-
513 fected by the particulars of different strains/species moving through elongation/retraction of an
514 appendage, we expect it to provide a relevant framework to study co-colonization in different me-
515 chanical micro-environments.

516 **Methods and Materials**

517 **Bacterial strains**

518 Strains used in this study were *Pseudomonas aeruginosa* wild-type (WT) PAO1, fluorescent strains
519 PAO1 miniCTX-PX2-gfp and PAO1 miniCTX-PX2-eyfp (a kind gift from PBRC group, IBS, Grenoble,
520 unpublished), and PAO1 mutants *pilA::Tn5*, *sadC::Tn5* and *wspR::Tn5* obtained from the transpo-
521 sion library at University of Washington (Jacobs *et al.*, 2003). Strain PAO1 pCdrA-gfp was obtained
522 by transforming plasmid *pCdrA::gfp^C* from (Rybtke *et al.*, 2012) in our WT strain.

523 Bacteria were inoculated in Luria-Bertani (LB) medium from glycerol stocks, and grown overnight at
524 37 °C at 250 rpm. The next morning, 10 µL of the stationary phase culture were diluted in 3 mL of LB
525 medium and placed in a shaking incubator (37 °C, 250 rpm) for 3.5 hours, to reach mid-exponential
526 phase ($OD_{600} = 0.6-0.8$). Bacteria were then diluted to $OD_{600} = 0.005$ in our working medium, TB:PBS,
527 and inoculated into the channel. TB:PBS is obtained by mixing TB (Tryptone broth, Euromedex,
528 10 g.L⁻¹) and PBS (w/o calcium and magnesium) with a volume ratio of 1:2. We found that this
529 minimal medium favors bacterial twitching for a few hours after adhesion.

530 **Microfluidic device**

531 Microfluidic channels were cut into 100 µm-thick double-sided sticky tape (7641W #25, Teraoka,
532 Japan) with a die-cutter. Typically, a 5 cm-long x 1 mm-wide channel was used to bind together
533 a rectangular glass coverslip bearing the hydrogel patches, and a flat 5 mm-thick slab of poly-
534 dimethylsiloxane (PDMS, Sylgard prepared by mixing crosslinker and monomer solutions 1:10 and
535 baking at 65°C for 1 hour). Two channels were stuck together to obtain a height of 200 µm, in order
536 for the flow through the channel to not be significantly modified by the 25 µm-thick PAA hydrogels.

537 These sticky-tape channels were first adhered onto the PDMS piece and then placed onto the de-
 538 hydrated hydrogels. To ensure proper binding, the whole device was placed under vacuum for 30
 539 minutes. Next, the channel was rinsed with TB:PBS (1:2) for a minimum of 1 hr, in order to rehy-
 540 drate the hydrogels. Medium was placed in a plastic container and withdrawn into the channel
 541 with a syringe pump (Harvard Apparatus, USA, 30 $\mu\text{L}/\text{min}$) to avoid the formation of bubbles.

542 **Gels and substrates preparation**

543 Hydrogels of polyacrylamide (PAA) and polyethyleneglycol (PEG) were prepared following previ-
 544 ously established protocols (*Tse and Engler, 2010; Beamish et al., 2010*). All reagents were ob-
 545 tained from Sigma Aldrich and used as received: Acrylamide solution (AA, 40% in water), N,N'-
 546 Methylenebisacrylamide (Bis, 2% in water), Ammonium Persulfate (APS, $\geq 98\%$), N,N,N',N'- Tetram-
 547 ethylethylenediamine (TEMED, $\geq 99\%$), Poly(ethylene glycol) diacrylate (PEGDA, $M_n \sim 6000 \text{ g}\cdot\text{mol}^{-1}$),
 548 2-Hydroxy-4'-(2-hydroxyethoxy)-2-methylpropiophenone (Irgacure 2959, 98%), Bind-silane, Sigma-
 549 cote.

550 Rectangular glass coverslips (24 \times 60 mm) were used as substrates for gel casting. They were
 551 plasma-cleaned and immersed in a solution of Bind-silane (60 μL of Bind-silane, 500 μL of 10 %
 552 acetic acid, 14.5 mL of ethanol) for 1 hour before being rinsed with ethanol, water, and blow-dried
 553 with nitrogen before use. Round glass coverslips (12 mm diameter) were used as counter-surfaces
 554 for gel casting. After plasma cleaning, they were immersed in Sigmacote for 1 hour before rinsing
 555 with acetone, ethanol and water, and blow-dried before use.

556 Bulk solutions of AA/Bis and PEGDA were prepared in phosphate buffer saline (PBS) and stored
 557 at 4 $^\circ\text{C}$ until use. The final stiffness of the gels was tuned by adjusting the AA/Bis or PEGDA content
 558 according to Table 1. PAA gels were obtained by adding 1 μL of TEMED and 1 μL of a freshly made
 559 APS solution (10 w% in water) to a volume of 168 μL of AA/Bis solution. A 3 μL droplet of the mix-
 560 ture was immediately placed on the surface of a bindsilane-treated glass coverslip, sandwiched by
 561 a Sigmacote-treated round coverslip, and left for curing for 1 hour in a water vapor-saturated atmo-
 562 sphere. After curing, the round coverslip was lifted off using the tip of a scalpel blade, resulting in a
 563 circular pad of gel, of thickness $\sim 25 - 30 \mu\text{m}$, covalently bound to the bottom rectangular coverslip
 564 and exposing its free top surface. Circular gel pads were then scrapped with a razor blade in order
 565 to adjust their lateral size to the width of the microfluidic channels into which they would eventu-
 566 ally be installed. Gel pads were then copiously rinsed with ultrapure water, and left for drying in a
 567 laminar flow cabinet. Up to three such pads, with different elastic properties, were prepared simul-
 568 taneously on the same coverslip, arranged to fit along the length of the microfluidic channel. PEG
 569 gels were obtained by adding 5 μL of a 10 wt% solution of Irgacure in ethanol to 0.5 mL of PEGDA
 570 solution. A 3 μL droplet of the mixture was placed in between coverslips as described above, and
 571 irradiated under UV light (365 nm, 180 $\text{mW}\cdot\text{cm}^{-2}$) for 15 minutes for curing. Subsequent steps were
 572 as described above for PAA gels.

Table 1. Hydrogel compositions and associated Young's moduli

Acrylamide (wt%)	Bis-acryl. (wt%)	PEGDA (wt%)	Modulus (kPa)
4	0.225	0.0	2.7 \pm 0.3
5	0.225	0.0	6.1 \pm 0.2
8	0.264	0.0	18.5 \pm 0.7
20	0.47	0.0	65 \pm 5.6
15	0.65	0.0	84 \pm 1.1
20	0.7	0.0	103 \pm 3.8
0	0	5	5.7 \pm 0.3
0	0	20	102 \pm 8.4

573 **Mechanical characterization**

574 The viscoelastic properties of the various gels were characterized by AFM microrheology, using the
575 “contact force modulation” technique described recently and validated on hydrogels (*Abidine et al.,*
576 **2015**). It allows determining elastic and loss shear moduli, G' and G'' , as a function of frequency
577 over the range 1 – 300 Hz. The Young moduli reported in table 1 have been computed as $E = 3G'_0$,
578 with G'_0 the low frequency plateau modulus obtained by microrheology, assuming a Poisson ratio
579 $\nu = 0.5$ for all gels. All gel samples displayed elastic behavior with $G' \gg G''$.

580 Measurements were performed on a JPK Nanowizard II AFM, with pyramidal-tipped MLCT probes
581 (Bruker) of spring constant 15 mN/m. Data were analyzed using a home-written software for mi-
582 corheology. 30 μ m-thick gels were prepared, as described above, on round coverslips mounted at
583 the bottom of 35 mm petri dishes. They were then either characterized immediately or left to dry
584 to mimic the protocol used for inclusion in the flow chamber. Experiments were performed in
585 PBS + 1 % vol. tween 20 (Sigma), with Tween used to prevent adhesion of the AFM tip to the gel. All
586 measurements were carried out at 37 °C to mimic experimental conditions with bacteria. Results
587 were compared with force-distance indentation curves that gave consistent results at low rigidities
588 (< 20 kPa) but overestimated the rigidity for higher values (Fig.1-fig. suppl. 1a).

589 Homogeneity of the gels was assessed at the μ m and mm scales by multiposition measurements.
590 We found very good repeatability of the measurements and homogeneity of the gels at all scales
591 (Fig.1-fig. suppl. 1b). Subsequent measurements were hence acquired at 3-6 different points in
592 the gels and the average and standard error of the mean are provided (Table 1). Rigidity was also
593 measured before and after drying and rehydration of the gel to check for possible damage to the
594 structure. In addition, confocal images of the surface of fluorescently labelled gels were used to
595 track default on the gel surface before and after drying. We found no evidence of damage to the
596 hydrogel upon drying, except for very soft gels of rigidity below 1 kPa that were not used in this
597 study (Fig.1-fig. suppl. 1c).

598 **Microscopy experiments**

599 Diluted bacterial solution was injected into the channel, and kept without flow for 30 min to allow
600 bacteria to attach. During that time, clean tubing was connected to a syringe and filled with TB-PBS
601 medium supplemented with 3 mM glucose and connected to the inlet of the device. 30 min after
602 injecting bacteria into the device, the flow of clean medium was initiated. The flow rate was first
603 set at 25 μ l/min for 3 min in order to flush out unattached bacteria, and then lowered to 1 μ L/min
604 and maintained constant with a syringe pump (Pico Plus, Harvard Apparatus) throughout the ac-
605 quisition (yielding a wall shear stress of 2.5 mPa). The set up was immediately placed into the
606 incubation chamber (37 °C) of a Leica SP8 confocal microscope, and acquisition was started at 1
607 frame/minute.

608 For matrix staining experiments, concanavalin A (Alexa Fluor 647 conjugate, ThermoFisher Scien-
609 tific) was added to the medium (3 μ l/ml of a 1mg/ml stock solution) and infused in the flow cell
610 for at least 30 min prior to imaging. Since the tetravalent conA interferes with the structure of the
611 matrix, it was used either for short-term imaging of bacterial twitching at early stages ($t < 1$ h, fig.
612 4D), or added at the end of an acquisition to assess matrix distribution on and around colonies
613 ($t \sim 8$ h, Fig.4-fig. suppl. 1).

614 For control experiments in wells (Fig. 1-fig. suppl. 3), the protocol was modified as follows: PAA
615 gels were prepared as described above, but at the center of a 35 mm round glass coverslip. The
616 coverslip was then glued (5-min epoxy, Araldite) to the bottom of the well of a 6-well plate (Costar,
617 Corning), previously cut-out to open a circular 32-mm hole. 1 mL of diluted bacteria suspension
618 ($OD_{600} = 0.005$) were deposited on the gel, incubated for 30 min, and then carefully pipetted out, and
619 the well was filled with 3 mL fresh medium (TB-PBS + 3 mM glucose) and kept at 37 °C. This setup
620 allowed continuous imaging of bacteria on a Zeiss Axio-observer 7 inverted microscope in phase
621 contrast mode (63x objective) equipped with an Orca-Flash 4.0 LT camera (Hamamatsu).

622

623 **Surface coverage analysis and tracking of individual bacteria**

624 All image processing and analysis, unless otherwise noted, was performed with Fiji using avail-
625 able plugins and home-written macros. In order to quantify the movements of individual bacteria,
626 time series of phase-contrast images were registered using the Fiji plugin "MultiStackReg" *Theve-*
627 *naz et al. (1998)* and segmented with the plugin "weka trainable segmentation" *Arganda-Carreras*
628 *et al. (2017)*. The resulting segmentation was checked and corrected manually.

629 For the analysis of the global velocity V_g , segmented binary images were used to estimate the sur-
630 face coverage $A(t)$ and the explored surface area $S(t)$, using a home-written MATLAB script. Briefly,
631 at each timepoint 2 binary images were generated: one where pixels occupied by bacteria were
632 assigned the value 1, and all others zero (providing $A(t)$), and another image obtained by adding
633 all binary images up to this timepoint, so that all visited pixels were assigned the value 1 (providing
634 $S(t)$).

635 For the analysis of individual displacement steps, segmented bacteria were fitted with an ellipse,
636 and the "analyze particle" imageJ function was subsequently used to locate the center of mass of
637 each bacterium. The Fiji plugin "TrackMate" *Tinevez et al. (2017)* was used to track all individual bac-
638 teria, again followed by manual validation and correction (see Video 2). The function importTrack-
639 MateTracks (<https://github.com/fiji/TrackMate/blob/master/scripts/importTrackMateTracks.m>) was
640 used to import tracking data into MATLAB, and homemade scripts were used to sort data, plot
641 tracks and obtain velocity distributions.

642
643 The analysis of the histograms of displacement steps were performed as follows: we assume
644 that the measured steps are the incoherent sum of two displacement vectors, the active displace-
645 ment \vec{V}_a due to T4P activity, and a vector \vec{V}_p that includes passive effects due to both the noise
646 on measurements, and displacements resulting from bacterial growth and local crowding. First,
647 we considered the experimental distribution obtained with the *pilA* mutant, for which $\vec{V}_a = \vec{0}$: this
648 allows extracting the probability distribution for $\|\vec{V}_p\|$, which can be well fitted with a decreasing
649 exponential with a characteristic passive velocity $V_{C,p}$: $p(\|\vec{V}_p\|) = \exp(-\frac{\|\vec{V}_p\|}{V_{C,p}})$, with $V_{C,p} = 0.044 \mu\text{m}/\text{min}$.
650 We then considered the case of twitching bacteria. Here, we observed that the tail of the displace-
651 ment step distribution also follows a decreasing exponential trend. Based on the reasoning that
652 passive displacements are short-ranged and should not significantly modify the distribution for
653 large displacement values, we deduce that the tail of the probability distribution for $\|\vec{V}_a\|$ is a de-
654 creasing exponential, $p(\|\vec{V}_a\|) = \exp(-\frac{\|\vec{V}_a\|}{V_C})$, with V_C the characteristic active twitching velocity of
655 bacteria.

656 We confirmed the validity of this hypothesis by calculating the probability distribution functions.
657 We assumed that the distribution of measured displacement steps, $\|\vec{V}_{tot}\| = \|\vec{V}_a + \vec{V}_p\|$ is the sum
658 of two uncorrelated exponential distributions with different scales and a random angle between
659 the two vectors. There is no analytical expression for this sum, hence we performed numerical
660 calculations of the distributions obtained in the general case. In the limit $\|\vec{V}_{tot}\| \gg V_C > V_{C,p}$ an
661 exponential distribution is retrieved with a characteristic velocity V_C , unaffected by $V_{C,p}$ (Fig. 3-fig.
662 suppl. 3, left). A fitting of the range $p(\|\vec{V}_{tot}\|) < 0.3$ (which excludes the first few points that do not
663 follow an exponential trend) confirms that V_C is obtained accurately provided that $V_C > V_{C,p}$ (Fig.
664 3-fig. suppl. 3, right). Below this limit, only $V_{C,p}$ is detected since active displacements are in the
665 range of passive "noisy" ones.

666 Experimentally, we have used a lower cutoff of $\|\vec{V}_{tot}\| > 0.08 \mu\text{m}/\text{min} \simeq 2V_{C,p}$ for the fitting range, to
667 restrict it to the exponential part of the distribution. To account for the noise in the measurement,
668 we have also considered that fitted values below $V_{C,p} = 0.044 \mu\text{m}/\text{min}$ were in the range $[0; 0.044]$
669 $\mu\text{m}/\text{min}$.

670 **Quantification of the morphology of colonies**

671 Quantification was performed on confocal fluorescence 3D resolved images. First, signal attenua-
672 tion with depth was compensated by decreasing exponential fitting of the mean pixel values inside
673 the colony with depth, and normalization by the corresponding function. A 2D 3x3 smoothing op-
674 eration was then performed on each image of the z-stack, and the colonies were subsequently
675 segmented using a simple thresholding operation: while this procedure does not permit segmen-
676 tation of individual bacteria, it provides a good estimate of the 3D envelope of the colonies. The
677 topology of the colonies was then quantified by calculating the roughness of this envelope using
678 the widely-used arithmetic average roughness Ra

$$Ra = \frac{1}{N} \sum_{i=1}^N |z_i - \langle z \rangle|, \quad (12)$$

679 where summation is over all 2D positions i in the 3D image, z_i is the height of the highest segmented
680 pixel at position i and $\langle \rangle$ is the averaging operator over all positions. The occupied volume V is
681 calculated as

$$V = p_x^2 \sum_{i=1}^N z_i, \quad (13)$$

682 with p_x the pixel size. The occupied area as a function from the distance to the coverslip is the his-
683 togram of z_i values with bin size $0.5 \mu\text{m}$ (corresponding to the vertical sampling of the 3D images).

684 **Quantification of the mixing of two strains co-colonizing the same soft substrate,**
685 **as a function of the softness**

686 This quantification is performed both at the low density stage with isolated bacteria, and at a later
687 stage on maturing colonies. To this aim, we used a statistical tool, Moran's I index, designed to
688 quantify the spatial clustering of species and widely used in the field of ecology and geography
689 **Moran (1950)**. Moran's I is a measure of the local spatial correlations that includes a notion of
690 spatial proximity, either in the form of a spatial cut-off for the calculation of the heterogeneity (in
691 other words, a characteristic distance), or a number of neighbors. It takes values ranging from
692 1 (perfectly correlated values) to -1 (perfectly anti-correlated values), with 0 corresponding to a
693 spatially random distribution of the variable.

694 Considering a variable y that can take two different values (in our case, green (1) or yellow (-1))
695 with n realisations, Moran's I is expressed as:

$$I = \frac{n}{\sum_{i=1}^n \sum_{j=1}^n w_{ij}} \frac{\sum_{i=1}^n \sum_{j=1}^n w_{ij} (y_i - \langle y \rangle) (y_j - \langle y \rangle)}{\sum_{i=1}^n (y_i - \langle y \rangle)^2}, \quad (14)$$

696 where w_{ij} is the matrix of weights that contains the spatial information (with $w_{ii} = 0$). In our ex-
697 periment, the relevant spatial scale (and hence the matrix of weights) varies greatly over time be-
698 cause of the change in the density of the bacteria on the surface. While at high density (maturing
699 colonies) defining a length scale is a suitable way of testing the presence of local correlations, this is
700 more challenging at earlier times when the distance between neighbours exhibits large stochastic
701 variations, in particular for stiff substrates. Hence, different matrices of weights were chosen for
702 early-stage and later-stage colonisation of the surface:

- 703 • at early stages of colonisation, when the bacteria are sparse on the surface, we chose to focus
704 on the nearest neighbours of each bacteria. To this aim, individual bacteria are segmented
705 in the green and yellow images, and their center of mass location is collated into a list of 2D
706 coordinates and colour for all bacteria in the field of view. Moran's I is then calculated based

707 on this list using the following weight matrix:

$$w_{ij} = \begin{cases} 1 & \text{if } j \text{ is one of the } p \text{ nearest neighbours of bacteria } i \\ 0 & \text{otherwise} \end{cases}$$

708 We arbitrarily chose $p = 5$ as a significant number of neighbours, although similar results are
709 found for values of p ranging from 4 to 10. Lower numbers are biased by cell division: at
710 the time of division, the closest neighbour is necessarily of the same strain as the bacteria
711 under consideration, so that there is always a positive correlation between them. As a result,
712 testing for mixing requires to mitigate this effect by choosing a large enough value for p . In
713 practice, we found that $p = 5$ was a good compromise to limit this bias while maintaining a
714 "local" approach, i.e. not considering the correlation between bacteria further apart than half
715 of the field of view (i.e. $160 \mu\text{m}$).

716 • at later stages with dense, 3D colonies, individual segmentation of bacteria becomes challeng-
717 ing and the correlation measure is performed on individual pixels: first, a simple thresholding
718 operation is performed on the green and yellow image, and each pixel is attributed a value:
719 1 (green pixel), 0 (black pixel) or -1 (yellow pixel). From this new image, Moran's I is calculated
720 using the following weight matrix:

$$w_{ij} = \begin{cases} 1 & \text{if the distance between } i \text{ and } j (i \neq j) \text{ is smaller than or equal to } d \\ 0 & \text{otherwise} \end{cases}$$

721 Again, the cut-off distance d is arbitrarily chosen as $5 \mu\text{m}$ although values between 3 and
722 $10 \mu\text{m}$ yield similar results: it permits limiting fluctuations by averaging over a significant
723 number of bacteria, while maintaining a local measure of mixing. In addition, because in-
724 dividual bacteria cover more than one pixel in the acquired images, a number of pixels of the
725 same colour as pixel i are removed to avoid correlating the bacteria with itself. In our data
726 the average number of pixels covered by one bacteria is measured to be 40.

727 While there is some degree of freedom on the choice of the weight matrix, it is important to
728 note that we use the same weight to compare data obtained on three different rigidities, hence
729 minimising the impact of the exact chosen parameters on the comparison. In contrast, values ob-
730 tained on one surface at the two different time points should not be directly compared as they
731 have not been obtained with the same weight matrix.

732

733 Acknowledgments

734 We thank Claude Verdier for help with the AFM elasticity measurements, Denis Bartolo for help
735 with microfluidics, and Benoit Coasne and Benedikt Sabass for fruitful discussions on data mod-
736 eling. We are extremely grateful to Ina Attree and Sylvie Elsen (IBS, Grenoble) for strains, help
737 and advice. We thank Tim Tolker Nielsen for the kind gift of pcdRA-gfp reporter plasmids. D.D.
738 was supported by the French National Research Agency (grant ANR-19-CE42-0010). The authors
739 acknowledge support from LabeX Tec 21 (ANR-11-LABX-0030).

Supplementary figures and Videos

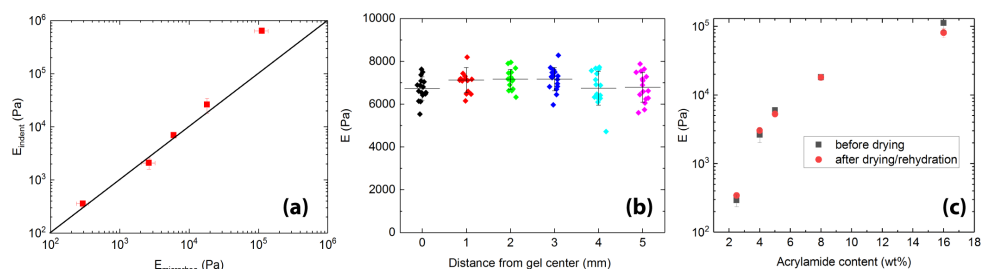


Figure 1-figure supplement 1: Mechanical characterization of hydrogels by AFM (a) comparison of elastic moduli measured by indentation and by microrheology. Both techniques yield quantitatively similar results for gels with Young's moduli $E < 20$ kPa. (b) spatial homogeneity of the gels characterized by indentation measurements. For each position, separated by 1 mm, a 4x4 force spectroscopy map is taken, with a spacing between "pixels" of $3\mu\text{m}$. (c) comparison of elastic moduli E measured before and after drying/rehydration of the gels.

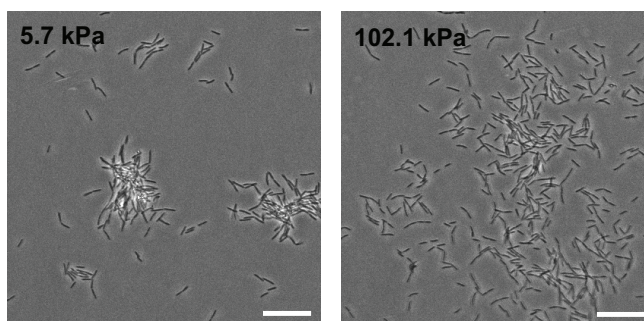


Figure 1-figure supplement 2: Morphology of microcolonies is strongly impacted by surface rigidity on PEG hydrogels. Phase contrast images of WT PAO1 bacteria on PEG hydrogels 5h after the onset of surface colonization. Scale bars, $20\mu\text{m}$.

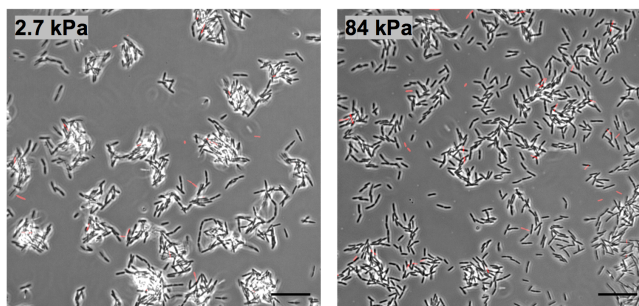


Figure 1-figure supplement 3: Substrate rigidity impacts early microcolony morphology in the absence of shear flow. Phase contrast images of WT PAO1 bacteria on PAA hydrogels at the bottom of a 6-well plate, after 150 min of incubation at 37°C without agitation. In red: initial adhering bacteria at t_0 . (Scale bars, $20\mu\text{m}$.)

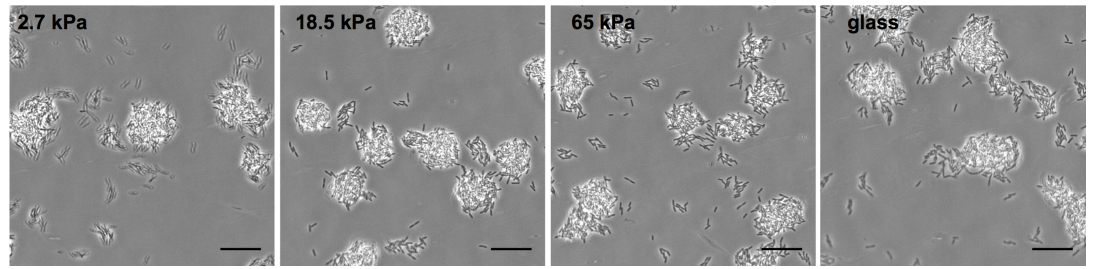


Figure 1-figure supplement 4: In the T4P-deficient mutant *PAO1 pilA::Tn5*, substrate rigidity does not significantly impact colony morphology. Colonies imaged after 5 h. Scale bar 20 μm .

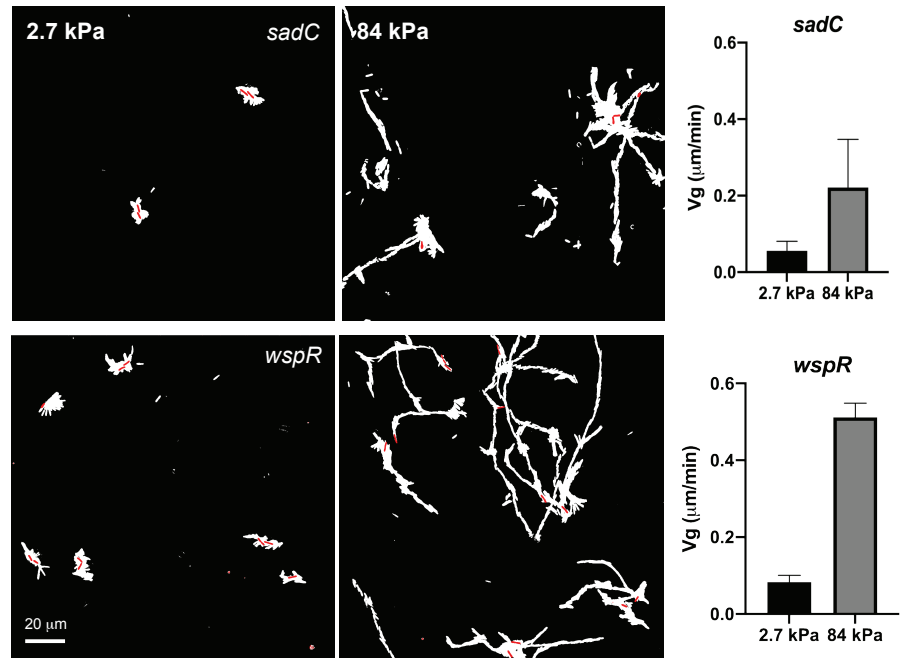


Figure 2-figure supplement 1: Behavior of mutants *PAO1 sadC :: Tn5* and *PAO1 wspR :: Tn5* on soft (2.7 kPa) and stiff (84 kPa) PAA hydrogels. Left: typical images showing initially attached bacteria (red) and total explored area after 100 minutes (white). Right: Average bacterial velocity V_g calculated using equation 2 of the main text, over the first 100 minutes of acquisition (1 experiment for each strain, 3 different positions for each gel. Error bars are SEM).

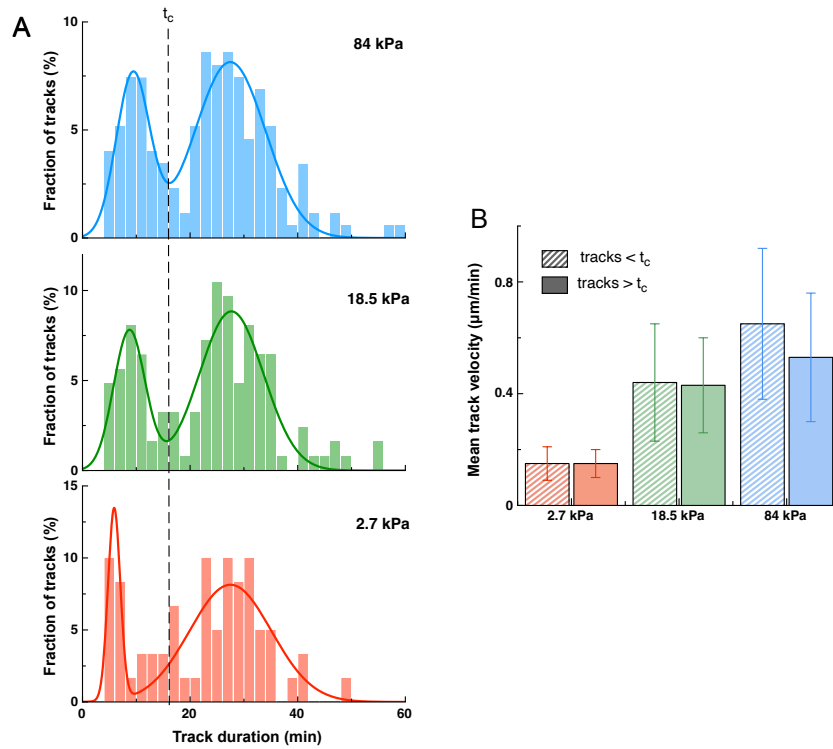


Figure 3-figure supplement 1: (A) Distribution of the path duration of bacterial tracks measured on different PAA substrates (WT PAO1). One track starts after a division event, and finishes either at the next division, or when the bacterium leaves the surface. Full lines are bimodal gaussian fits, evidencing a sub-population of bacteria that detach from the surface before dividing. (B) Mean track velocity is similar for short tracks (below the cutoff value $t_c=16$ min) and long tracks, for all tested substrate rigidities. (total number of analyzed tracks: 60 (2.7 kPa), 124 (18.5 kPa), 175 (84 kPa)).

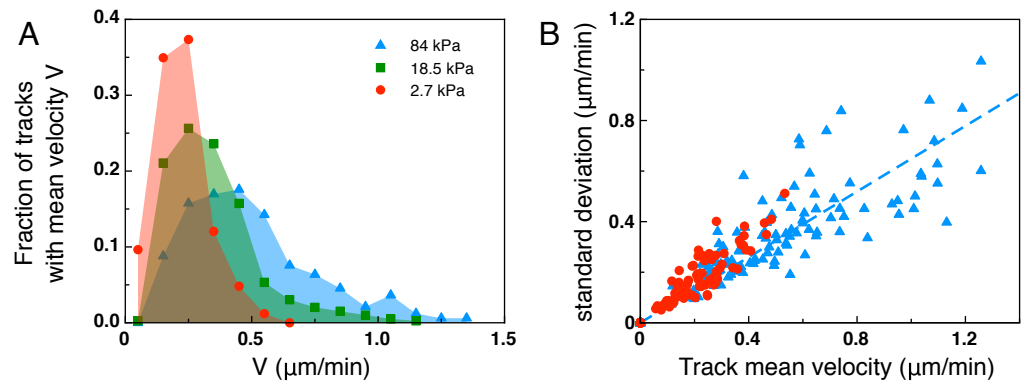


Figure 3-figure supplement 2: Analysis of the mean track velocity. (A) Mean track velocity distribution for different values of the substrate rigidity. Only full tracks were considered (corresponding to the right peak in Fig.7). Considering all tracks does not significantly modify the distributions (data not shown). 84 kPa: 330 tracks from 2 independent experiments, 18.5 kPa: 394 tracks from 3 independent experiments, 2.7 kPa: 83 tracks from 2 independent experiments. (B) Standard deviation of the mean velocity for individual tracks, shown for the 2.7 kPa and 84 kPa data sets. Dotted line is a linear fit for the 84 kPa data ($y=0.65x$).

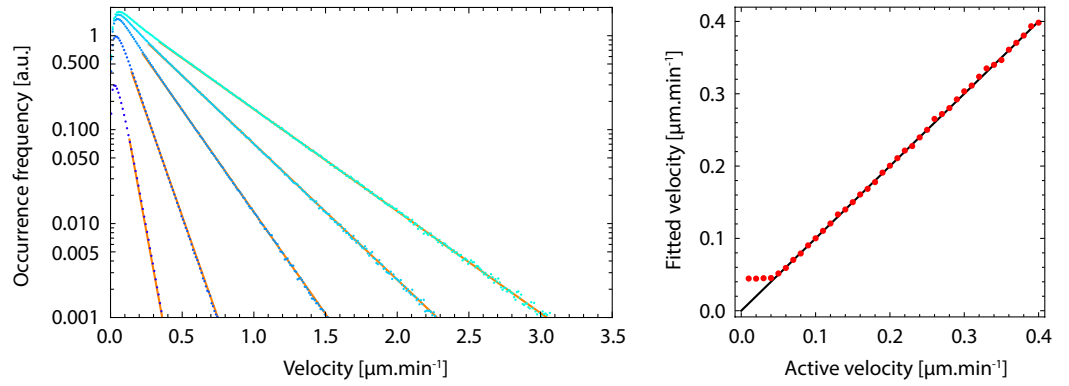


Figure 3-figure supplement 3: Validation of the fitting of displacement steps distributions with single exponentials. Left, calculated distributions (dots) of the sum of two uncorrelated random vectors each following a decreasing exponential distribution with characteristic velocities V_C and $V_{C,p}$ at an angle following a random distribution. $V_{C,p} = 0.044\mu\text{m}/\text{min}$ is equal to the experimentally measured value on the *pilA* mutant. V_C spans a range similar to experimental measurements, (0.05, 0.1, 0.2, 0.3 and $0.4\mu\text{m}/\text{min}$, from dark blue to cyan). Orange lines are exponential functions with the corresponding V_C . Right, characteristic velocities extracted by fitting the exponential part of the simulated distributions, as a function V_C , with $V_{C,p} = 0.044\mu\text{m}/\text{min}$. The black line corresponds to $y=x$.

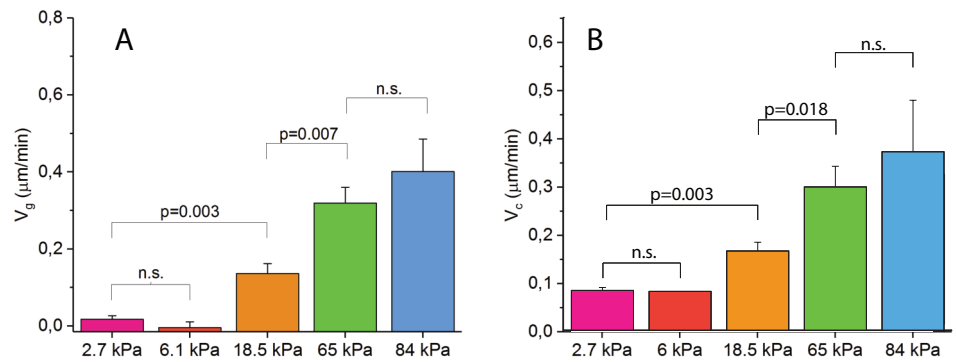


Figure 3-figure supplement 4: Statistical analysis of V_g (A) and V_c (B) for various gel rigidities. Indicated are p-values from paired two-sided Mann-Whitney non-parametric tests. n.s. denotes datasets that are not significantly different at a threshold of 0.05.

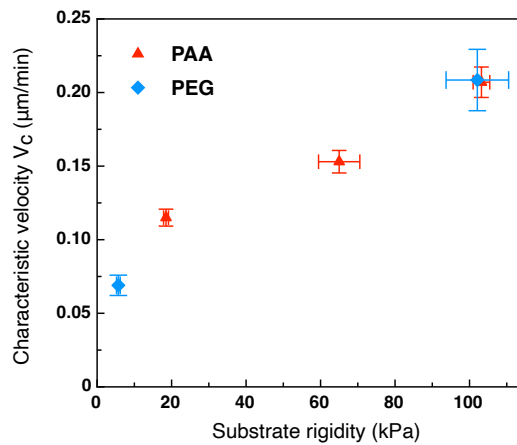


Figure 3-figure supplement 5: Characteristic twitching velocity measured on PEG hydrogels is similar to the one measured on PAA hydrogels under identical experimental conditions. V_C obtained by fitting the distribution of displacement steps on PAA or PEG hydrogels in a similar range of substrate rigidity. Error bars are SEM. Each point is the average of 2 positions from 1 experiment. (Note that for technical reasons these experiments were carried out with a wall shear stress of 6.4 mPa, about 3x higher than all other experiments on PAA).

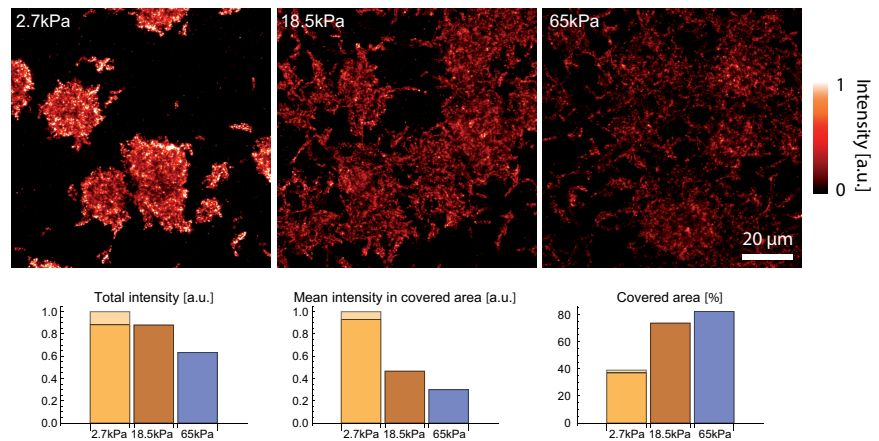


Figure 4-figure supplement 1: EPS staining with concanavalin A highlights matrix deposits on the surface of substrates of different stiffnesses after 8h of surface colonization. Matrix deposits are more compact on soft substrates with large areas (>60%) devoid of EPS, while stiffer substrates are almost fully decorated (>% covered area). The two colours for the softer surface corresponds to two areas taken 30 minutes apart after staining, before and after acquisition of the two other datasets on larger rigidities, to rule out any significant time evolution of the staining.

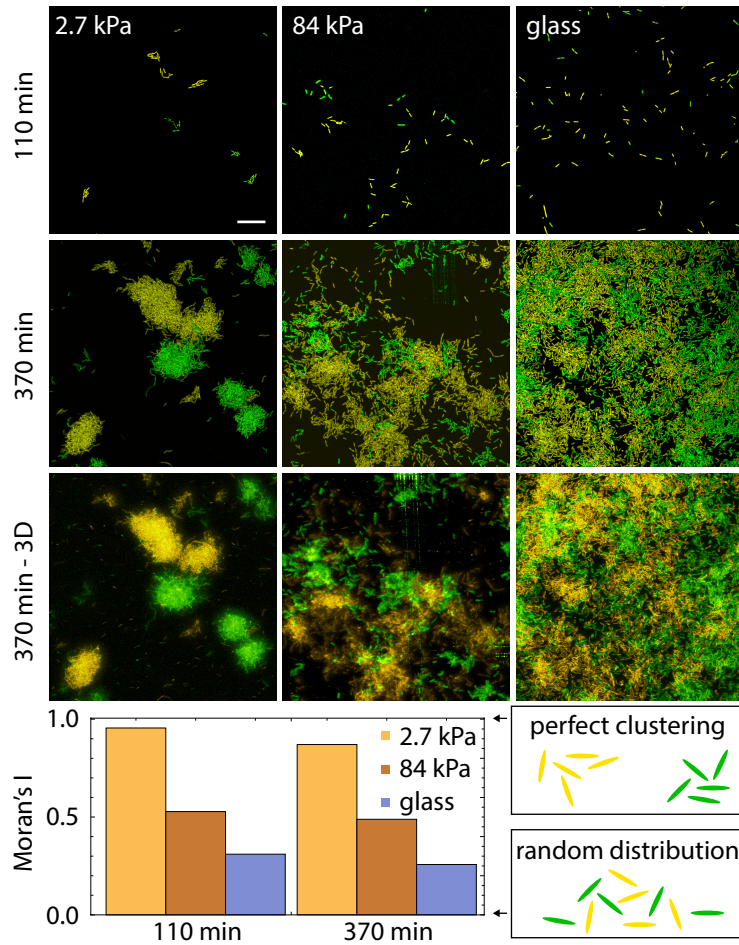


Figure 5-figure supplement 1: Bacterial spatial distribution as a function of substrate rigidity. Top, images of surfaces seeded with a 1:1 mixture of constitutively fluorescent bacteria expressing GFP or YFP at two different times after the start of surface colonization (bottom : 3D rendering of a volumetric image). Bottom, Spatial autocorrelation quantified via Moran's I at the two time points illustrated above. The values should not be directly compared between the two time points (see SI I-C) but illustrate that the rigidity modulation of mixing is maintained over time from very sparse to large coverage of the surface.

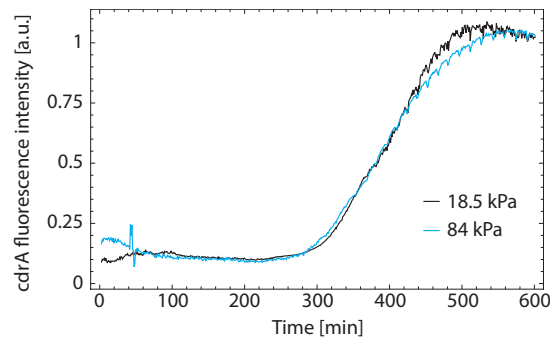


Figure 6-figure supplement 1: Fluorescence intensity from a PAO1 strain expressing a $P_{cdrA} - gfp$ plasmid over time, showing a plateau of fluorescence expression after ≈ 500 min. In our experiments, this change in behaviour might be due to a lack of oxygen in the flow upon growth of the biofilm in the microfluidic channel and occurs. Two rigidities are shown and scaled to the same final fluorescence value.

741 **Video 1** : surface colonization on 2.7 kPa (left) and 65 kPa (right) PAA hydrogels, imaged with
742 phase contrast microscopy with one image/min over 6 hours. The two gels were included in the
743 same microfluidic channel and imaged quasi-simultaneously. Scale bar, 20 μ m.

744

745 **Video 2** : Principle of the image processing for the tracking of individual bacteria. Glass sur-
746 face colonization under controlled shear flow followed over 90 minutes (1 frame/minute) by phase
747 contrast microscopy. Left, the registered phase contrast image is superimposed with the center
748 of mass of the detected cells after segmentation (green dots). Right, tracks of the detected cells
749 (obtained with the simple LAP tracker of the Trackmate ImageJ plugin), color-coded as a function
750 of the track final length. Scale bar, 20 μ m.

Appendix 1: Modeling twitching velocity on soft substrates

The principle of our modeling of rigidity-modulated twitching in 1D is shown in figure 2D (main text), and incorporates three main ingredients: modeling of the substrate deformation (subsection A), of cell body friction on the surface (subsection B) and of the pilus retraction dynamics (subsections C and D).

A. Modeling substrate deformation

We have based our approach on the theory of linear elasticity for the description of the substrate: in this framework, the deformation of the substrate occurs over a typical length scale given by the size of the adhesion, λ , and it is proportional to the applied force. Finally, the proportionality coefficient Y scales as the product of the substrate elastic modulus, E , and the adhesion size λ , i.e. $Y = E\lambda$. This simple relation is valid only for small displacements on rigid substrates. It is likely to fail quantitatively on very soft substrates with large displacements, low cross-linker densities and non-affine deformations, but is a reasonable first approximation for the simple model we propose here.

This modeling introduces characteristic length scales that depend on the part of the bacteria under consideration: both the pilus and the cell body form contact with the substrate. The pilus attaches at its tip over size $\lambda \approx 1$ nm, while the cell body has a typical size of $l_b \approx 1\mu\text{m}$. In addition, a third length scale is the typical length of the pilus, L , which varies during retraction but is most of the time $> 1\mu\text{m}$. Introducing these three quantities permits to simplify the description of the deformation of the substrate: the pilus tension F and the displacement at the adhesion site in the substrate u are linearly related by $F = Yu$, with Y being an effective spring constant. We model the substrate as an infinite (thickness $\approx 25\mu\text{m} \gg \lambda$, lateral extension $\approx 1 - 10\text{mm} \gg \lambda$), isotropic, elastic and incompressible half space. Furthermore, we neglect the influence of the cell body on the deformation around the pilus tip since $L \gg \lambda$ so that the deformation of the substrate has decayed to zero at the cell body.

The 2D Boussinesq Green's tensor at the surface $z = 0$ for a point-like shear force \mathbf{f} at the origin is given by *Landau and Lifschitz (2004)*

$$\mathbf{G}(\mathbf{r}) = \frac{3}{4\pi E} \left[\frac{\mathbf{I}}{r} + \frac{\mathbf{r} \otimes \mathbf{r}}{r^3} \right] \mathbf{f}. \quad (\text{A1})$$

Considering an adhesive T4P tip of length λ and half-width d and using slender body approximations, the total force F on the pilus for a "lengthside" displacement u is given by

$$F = \frac{E\lambda\pi}{3 \ln \frac{\lambda}{d}} u \quad \text{with} \quad Y = \frac{E\lambda\pi}{3 \ln \frac{\lambda}{d}} \approx E\lambda. \quad (\text{A2})$$

Here we have implicitly introduced a 1D setting, i.e. we will neglect the vectorial nature of forces and displacements and restrict ourselves to a 1D setting. We find, as expected, that Y scales linearly with λ . This holds equivalently for the cell body by replacing λ with $l_b \gg \lambda$: as a result, the substrate deformation at the cell body caused by the same pilus tension F is of amplitude smaller by a factor $\lambda/l_b \ll 1$ and will be neglected for the sake of simplicity.

In contrast, we consider the pilus tip to be firmly attached to the substrate until detachment while the cell body can slide on the surface. Note that this asymmetry between bacterial body (macroscopic sliding over the substrate) and the supposedly small pilus/substrate contact (point-like force deforming the substrate) is the essential difference to the pulling process described in Ref. *Simsek et al. (2019)*, where the contact of the bacterial body and the pilus extremity are mechanically treated as equivalent.

B. Modeling cell body friction

As stated above, the model requires a description of the sliding motion of the cell body on the substrate as a function of the force F applied by the pilus. We base our modeling on the theory from

794 **Sens (2013)** that considers stochastic friction by an ensemble of N elastic linkers (not necessarily
 795 all bound at all times) between an elastic substrate and a cell, submitted to a sliding velocity v . The
 796 bonds are modeled as slip bonds with a critical force f^* , an off-rate constant at zero force k_{off}^0 and
 797 an on-rate constant k_{on} . The linkers' stiffness is k_b .

798 In the case of an infinitely rigid substrate, the mean total force on the cell body $\langle F \rangle$ as a function
 799 of its velocity v is non-monotonous and is given by

$$\langle F \rangle = N f^* \frac{r_{\text{on}} e^{1/\tilde{v}} \int_0^\infty f e^{-\left(\frac{ef}{\tilde{v}}\right)} df}{\tilde{v} + r_{\text{on}} e^{\left(\frac{1}{\tilde{v}}\right)} \Gamma\left[0, \frac{1}{\tilde{v}}\right]} \quad (\text{A3})$$

800 with $\tilde{v} = v/v_\beta$, $v_\beta = k_{\text{off}}^0 f^*/k_b$, $r_{\text{on}} = k_{\text{on}}/k_{\text{off}}^0$. $\Gamma[0, x]$ is the Euler gamma function. Eq. (A3) exhibits a
 801 complex dependence of $\langle F \rangle$ on \tilde{v} that requires estimating typical values of the parameters in our
 802 experiments. Putting in numbers to obtain the typical speed v_β , we can estimate that

- 803 • $k_{\text{off}}^0 \approx 1 - 10 \text{ s}^{-1}$ (slightly higher than for specific ligand/receptor bonds **Robert et al. (2007)**)
- 804 • $f^* = k_B T/x_\beta$ with $x_\beta \approx 0.1 - 10 \text{ nm}$ being the transition state distance between bound and
 805 unbound state as proposed by Evans **Evans (2001)** and others **Pereverzev et al. (2005)**.
- 806 • k_b is more difficult to estimate. Here we assume that bacterial adhesion is mediated by the
 807 bacteria produced extracellular matrix, of which a major constituent are exopolysaccharides.
 808 Using a worm-like chain (WLC) model for a polymer of persistence length $L_p \approx 10 \text{ nm}$ (as
 809 calculated for bacteria produced exopolysaccharides in **Kuik et al. (2011)**) and contour length
 810 $L_0 \approx 100 \text{ nm}$ (assuming a chain length of about 100 monomers with size 1 nm), the linear
 811 force-elongation relationship in the regime of weak forces **Marko and Siggia (1995)** yields a
 812 force constant $k_b \approx \frac{3kT}{2L_p L_0} \approx 6 \times 10^{-3} \text{ pN.nm}^{-1}$.

813 Taking extreme values this leads to typical velocities in the range $v_\beta = 1 - 100 \mu\text{m.s}^{-1}$. In our experi-
 814 ments the bacteria are not expected to move faster than the pilus retraction velocity (i.e. $1 \mu\text{m.s}^{-1}$
 815 **Skerker and Berg (2001)**, if one excepts the case of slingshots that were not frequently observed in
 816 our experiments). Taking into account that the pilus retraction speed slows down considerably as
 817 the tension in the pilus increases, the bacterial speed during one pilus retraction is rather smaller
 818 than this maximum value. Hence, we always have $\tilde{v} = v/v_\beta < 1$, and Eq. (A3) can be linearized to

$$\langle F \rangle = N f^* \frac{k_{\text{on}}}{k_{\text{off}}^0 + k_{\text{on}}} \tilde{v}, \quad (\text{A4})$$

819 In addition, the elasticity of the substrate should be considered. Ref. **Sens (2013)** proposes that
 820 this situation is equivalent to having a system of springs in series, one stemming from the substrate
 821 elasticity and the second being the collection of individual bond springs (in parallel). In this case
 822 and using once again the theory of linear elasticity, the previous analysis holds if \tilde{v} is rescaled by a
 823 factor $\frac{E l_b}{k_b + E l_b}$, with $E > 3 \text{ kPa}$ the substrate Young's modulus and $l_b \approx 1 \mu\text{m}$ the characteristic size of
 824 the bacterial cell body, $a = l_b \approx 1 \mu\text{m}$. Hence $E l_b \geq 3 \text{ pN.nm}^{-1} \gg k_b$ and the scaling factor $\frac{E l_b}{k_b + E l_b} \approx 1$,
 825 so that the elasticity of the substrate does not influence the friction of the cell body.

826 In summary, we find that we can reasonably use a linear approximation for the bacterial sliding
 827 speed in response to the pulling force due to the pilus retraction, $F = \eta v$ with η a friction coefficient.
 828 Finally, we consider η as independent from the substrate rigidity, which is reasonable if we assume
 829 that the number of bonds is limited by the number of molecules/appendages of the cell body that
 830 can interact with the substrate, rather than the number of binding sites on the substrate itself
 831 (PAA mesh size $\approx 3 - 10 \text{ nm}$), and that the interaction may in addition be mediated by adsorbed
 832 exopolysaccharides deposited by the bacteria. However, other non-linear dependencies can be
 833 easily included into the modeling.

834 C. Basic modeling of pilus retraction

835 The relevant step during twitching which induces bacterial motion is the active pilus retraction
 836 when attached to the substrate. Here we assume, that the limiting effect for bacterial motion is
 837 the detachment of the pilus from the substrate, and not the complete retraction of the pilus by
 838 the bacterium. To understand the role in substrate rigidity on the bacterial twitching speed we will
 839 therefore concentrate on this crucial step without describing the whole cycle of pilus dynamics, for
 840 which the kinetics is not completely understood *Koch et al. (2021)*; *Talà et al. (2019)*.

841 We consider the retraction of a single effective pilus pulling on the bacterial body until it de-
 842 taches from the substrate. We treat the pilus as rigid and inextensible filament: assuming a force
 843 constant of $2 \text{ pN} \cdot \mu\text{m}^{-1}$ for the pilus elasticity *Beaussart et al. (2014)*, a substrate rigidity of $E =$
 844 100 kPa , an adhesion size of $\lambda = 1 \text{ nm}$ and a maximum force exerted by the pilus of $F_R = 100 \text{ pN}$,
 845 the substrate displacement is $u \sim F_R/E\lambda = 1 \mu\text{m}$. In contrast, the pilus elongation is $\Delta L = 50 \text{ nm}$
 846 and can therefore be neglected for our conditions. However it would not pose any difficulty to
 847 include the pilus elasticity into the calculations.

848 Let v_R be the retraction speed of the attached pilus inducing a displacement u in the substrate.
 849 At the same time the bacterium will slide forward with speed v_B , reducing the tension in the pilus
 850 and the displacement in the substrate:

$$\frac{du}{dt} = v_R(F) - v_B(F) \quad \text{with} \quad F = Yu. \quad (\text{A5})$$

851 Both motions (substrate displacement and bacterial sliding) are coupled via the tension in the pilus
 852 F . Its retraction speed is described by a simple linear dependence that has been well documented
 853 *Marathe et al. (2014)*; *Koch et al. (2022)*

$$v_R = v^0 \left(1 - \frac{F}{F_R} \right), \quad (\text{A6})$$

854 with F_R a stall force. As established in the previous subsection, the bacterial sliding speed depends
 855 linearly on the pilus tension with friction constant $\eta = F_B/v^0$:

$$v_B = \frac{1}{\eta} F = v^0 \frac{F}{F_B}. \quad (\text{A7})$$

856 F_B denotes the force necessary to pull the bacterium at maximum retraction speed v^0 over the
 857 substrate. From Eq. A5 we recover the increase in the pilus tension over time during the retraction

$$F(t) = F_0 \left(1 - e^{-\frac{Yv^0}{F_0}t} \right) \quad (\text{A8})$$

858 with the force scale

$$F_0 = \frac{F_B F_R}{F_R + F_B}. \quad (\text{A9})$$

859 Incorporating solution (A8) into Eq. (A7) with $v_B = \frac{dx_B}{dt}$ we recover for the bacterial sliding distance
 860 during pilus retraction

$$x_B(t) = \frac{F_0}{F_B} \left[v^0 t + \frac{F_0}{Y} \left(e^{-\frac{Yv^0}{F_0}t} - 1 \right) \right]. \quad (\text{A10})$$

861 While retracting the pilus will detach with a rate constant $k_{\text{off}}(F)$ from the substrate. Assuming a
 862 force independent off-rate constant $k_{\text{off}} = k_{\text{off}}^0$ the detachment times are distributed exponentially
 863 with mean $1/k_{\text{off}}^0$. Furthermore, we assume that the single effective pilus considered in our model
 864 retracts with frequency k_p and thus gives rise to an effective velocity

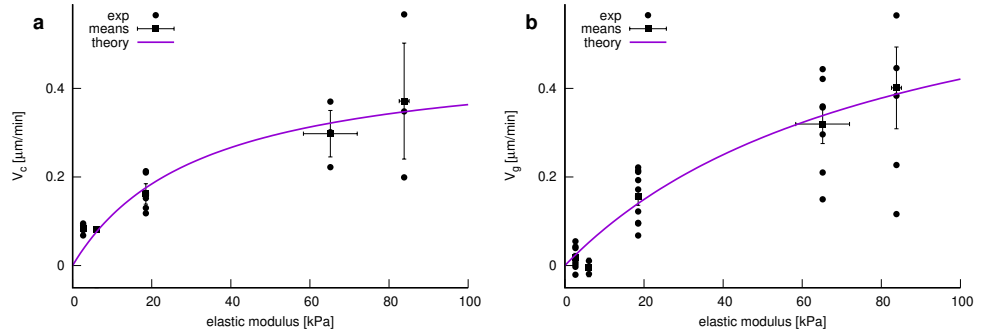
$$v_{\text{eff}} = k_p \langle x_B \rangle = k_p k_{\text{off}}^0 \int_0^\infty x_B(t) e^{-k_{\text{off}}^0 t} dt = V_{\text{max}} \frac{E}{E + E_0}. \quad (\text{A11})$$

865 Here, $\langle x_B \rangle$ denotes the mean bacterial sliding distance per pilus retraction event. V_{max} denotes the
 866 maximum effective speed that a cell can reach on a given substrate at infinite rigidity, given by

$$V_{\text{max}} = v^0 \frac{k_p}{k_{\text{off}}^0} \frac{F_R}{F_B + F_R}. \quad (\text{A12})$$

867 E_0 denotes the rigidity at half-maximal speed and is given by

$$E_0 = \frac{F_B F_R k_{\text{off}}^0}{(F_B + F_R) v^0 \lambda}. \quad (\text{A13})$$



Appendix 1-figure 1: Experimentally measured velocity vs. rigidity data and least squared fits of Eq. (A11) w.r.t. to the experimental values as indicated in the legends. a: Local velocity measures. Parameters obtained by a least-square fit: $E_0 = 32 \pm 20$ kPa, $V_{\text{max}} = 0.48 \pm 0.12$ $\mu\text{m}\cdot\text{min}^{-1}$. b: Global velocity measures. Parameters obtained by a least square fit: $E_0 = 84 \pm 68$ kPa, $V_{\text{max}} = 0.77 \pm 0.35$ $\mu\text{m}\cdot\text{min}^{-1}$. Errorbars indicate SEM.

868 Appendix 1-figure 1 shows the experimental data and fitted curves, which capture well the
 869 data for medium and high rigidities. The theoretical curves were fitted to all experimental values
 870 (applying the statistical weight in the measured rigidities and equal weight in the velocities) using a
 871 least square fit (software gnuplot *Williams et al. (2019)*). Assuming a typical pilus retraction speed
 872 $v^0 = 0.5 - 1$ $\mu\text{m}\cdot\text{s}^{-1}$ *Marathe et al. (2014); Koch et al. (2022)*, a stall force of the order $F_R = 50 - 100$ pN
 873 *Marathe et al. (2014); Koch et al. (2022)*, a pilus off-rate constant $k_{\text{off}}^0 = 1$ s^{-1} *Talà et al. (2019)* and
 874 a contact size of $\lambda = 1$ nm *Koch et al. (2022)*, a high friction surface with $F_B = 1$ nN and a typical
 875 pilus retraction frequency² of $k_p = 0.1 - 0.2$ s^{-1} we recover a $V_{\text{max}} \sim 0.1 - 1$ $\mu\text{m}\cdot\text{min}^{-1}$ and a substrate
 876 rigidity at half maximum speed of $E_0 = 10 - 100$ kPa, a range which encloses the fitted values (see
 877 Appendix 1-figure 1).

878 Here we have assumed a force-independent off-rate constant for the pilus. In a more complex
 879 scenario, the contact between the pilus and the substrate may act as a slip bond or catch bond. For
 880 completeness we will show some numerical results for slip and catch bond behavior below, which
 881 do not increase however the quality of fit between experimental and theoretical velocity data.

882 D. Force dependent detachment rate constants

883 Increasing the complexity of the model, we assume that the pilus detachment rate is force dependent
 884 *Kramers (1940); Bjørnham and Axner (2010); Pereverzev et al. (2005); Talà et al. (2019)* and
 885 takes the form

$$k_{\text{off}} = k_{\text{off}}^0 \left(\epsilon e^{-\frac{F}{F_C}} + e^{\frac{F}{F_S}} \right). \quad (\text{A14})$$

886 $\epsilon = 0$ denotes a slip bond and $\epsilon > 0$ denotes a catch bond behavior. F_C and F_S denote positive
 887 force constants *Pereverzev et al. (2005)*. Eq. (A14) implies that the pilus detachment times are not
 888 distributed exponentially.

889 We now consider the evolution equation for the probability density $p(u)$ that a pilus attached to
 890 the substrate is retracting and is thereby inducing a displacement u

$$\partial_t p = -k_{\text{off}}(F)p - \partial_u j_u \quad (\text{A15})$$

891 The first term denotes (tension dependent) pilus detachment from the substrate and the second
 892 term captures the advection of the displacement due to pilus retraction and bacterial sliding. It is

²Here we assume that one single effective pilus is active during a retraction event. Using a typical pilus length of 5 μm with retraction speed of $v_0 = 0.5 - 1$ $\mu\text{m}\cdot\text{s}^{-1}$ gives a duration of 5-10 s per retraction and a retraction frequency of $0.1 - 0.2$ s^{-1}

893 formulated as a divergence of a flux j_u with

$$j_u = [v_R(F) - v_B(F)] p. \quad (\text{A16})$$

894 The pilus retraction $v_R(F)$ and bacterial sliding speed $v_B(F)$ is given by Eqs. (A6) and (A7). To facilitate
895 the analysis of the equations we use the transformation $p(u) = p(u[F]) = P(F)$ and $\partial_u = Y\partial_F$ which
896 gives rise to the evolution equation

$$\partial_t P(F) = k_{\text{off}}(F)P - v^0 Y \partial_F \left[\left(1 - \frac{F}{F_R} - \frac{F}{F_B} \right) P \right] \quad (\text{A17})$$

897 To reduce the number of parameters we introduce the timescale $t_0 = 1/k_{\text{off}}^0$, the length scale $l_0 =$
898 $v^0 t_0$ and the force scale $F_0 = (F_R F_B)/(F_R + F_B)$. The adimensional quantities are then denoted
899 $\tilde{F} = F/F_0$, $\tilde{t} = t/t_0$, and $\tilde{u} = u/l_0$. The adimensional evolution equation of $\tilde{P}(\tilde{F})$ takes the form

$$\partial_t \tilde{P} = -\kappa(\tilde{F})\tilde{P} - \mu \partial_{\tilde{F}} [\tilde{P}(1 - \tilde{F})], \quad \text{with } \tilde{F} \in [0, 1] \quad (\text{A18})$$

900 where $\mu = Y v^0 / (F_0 k_{\text{off}}^0)$ denotes the adimensional substrate rigidity and κ denotes an adimensional
901 force dependent off-rate, i.e. $\kappa = k_{\text{off}} / k_{\text{off}}^0$. Solving Eq. (A18) in the steady state we find

$$\tilde{P} = \frac{\tilde{P}_0}{1 - \tilde{F}} e^{\frac{\mu \tilde{F}}{\mu}} \quad (\text{A19})$$

902 with

$$I(\tilde{F}) = \varepsilon e^{-\frac{1}{\tilde{F}_C}} \text{Ei} \left(\frac{1 - \tilde{F}}{\tilde{F}_C} \right) + e^{\frac{1}{\tilde{F}_S}} \text{Ei} \left(-\frac{1 - \tilde{F}}{\tilde{F}_S} \right). \quad (\text{A20})$$

903 In Eq. (A20) the force constants \tilde{F}_C and \tilde{F}_S have been rescaled by F_0 . The normalization factor
904 P_0 is defined by the integral condition $\int_0^1 \tilde{P}(\tilde{F}) d\tilde{F} = 1$. $\text{Ei}(x)$ denotes the exponential integral. At
905 detachment the distribution of forces \tilde{F}_d is given by

$$\tilde{P}_d(\tilde{F}_d) = \tilde{P}_{d0} \frac{\kappa(\tilde{F}_d)}{1 - \tilde{F}_d} e^{\frac{\mu \tilde{F}_d}{\mu}} \quad (\text{A21})$$

906 with the normalization factor \tilde{P}_{d0} determined by the integral condition $\int_0^1 \tilde{P}_d(\tilde{F}_d) d\tilde{F}_d = 1$.

907 Using the forces and bacterial sliding distance at detachment from the substrate

$$\tilde{F}_d = 1 - e^{-\mu \tilde{t}_d} \quad (\text{A22})$$

$$\tilde{x}_B = \frac{1}{\tilde{F}_B} \left[\tilde{t}_d + \frac{1}{\mu} (e^{-\mu \tilde{t}_d} - 1) \right] \quad (\text{A23})$$

908 we can perform the transformation $\tilde{P}_d(\tilde{F}_d) d\tilde{F}_d = \tilde{P}_d[\tilde{F}_d(\tilde{t}_d)] \mu e^{-\mu \tilde{t}_d} d\tilde{t}_d = \tilde{P}_d(\tilde{t}_d) d\tilde{t}_d$ and recover the
909 mean bacterial displacement per pilus retraction in adimensional form as

$$\langle \tilde{x}_B \rangle = \int_0^\infty \tilde{x}_B(\tilde{t}_d) \tilde{P}_d(\tilde{t}_d) d\tilde{t}_d. \quad (\text{A24})$$

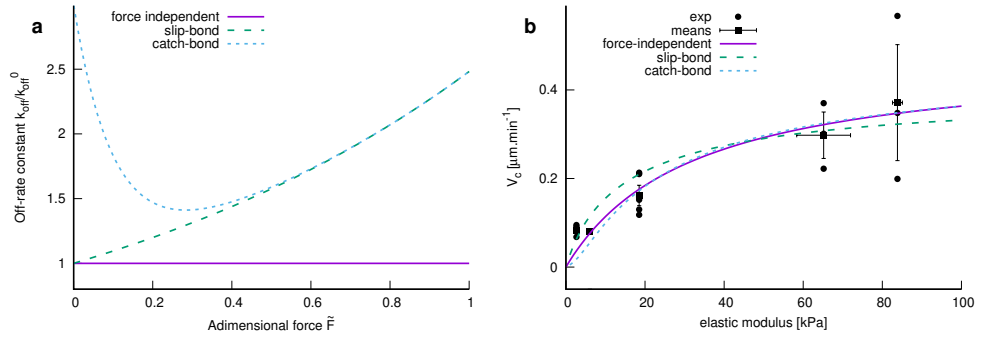
910 Following the same argument as for Eq. (A11), the effective bacterial speed (dimensional) is then
911 given by

$$v_{\text{eff}} = k_p l_0 \langle \tilde{x}_B \rangle = \frac{k_p}{k_{\text{off}}^0} v^0 \langle \tilde{x}_B \rangle \quad (\text{A25})$$

$$= V_{\text{max}} \int_0^\infty \left[\tilde{t}_d + \frac{1}{\mu} (e^{-\mu \tilde{t}_d} - 1) \right] \tilde{P}_d(\tilde{t}_d) d\tilde{t}_d, \quad (\text{A26})$$

912 with $\mu = E/E_0$.

913 Appendix 1-figure 2 shows exemplarily the off-rate constants for force independent, slip and
914 catch bond behavior (Appendix 1-figure 2a) and the effective velocity of a slip-bond and catch-
915 bond model along with a force independent detachment in comparison to the measured bacterial
916 velocity using the local velocity analysis (Appendix 1-figure 2b). Thereby we chose arbitrarily a slip-
917 bond constant $F_s = 1.1 F_0$ corresponding for example to the case of a high friction substrate with



Appendix 1-figure 2: Comparison of various force dependencies of the pilus detachment rate constant k_{off} as indicated in the legend. b: Comparison of bacterial velocities obtained by models with various complexity with experimentally measured values (local velocity analysis) as indicated in the legend (parameters were fit w.r.t experimental mean values). The model parameters for the force-independent model are as in Appendix 1-figure 1a. For the slip and catch bond model the fixed parameters are $E_0 = 32$ kPa, $\tilde{F}_S = 1.1$, $\epsilon = 2$ (catch bond), $\tilde{F}_C = 0.1$ (catch bond). For the slip and catch bond model V_{max} was estimated from least square fits: $V_{max} = 0.98 \mu\text{m}\cdot\text{min}^{-1}$ (slip) and $V_{max} = 1.15 \mu\text{m}\cdot\text{min}^{-1}$ (catch). Error estimates are expected to be of the same order of magnitude as for the force independent model (see Appendix 1-figure 1a).

918 $F_R = F_S = F_B/10$, i.e. as used previously $F_R = F_S = 100$ pN and $F_B = 1$ nN. The catch-bond force
 919 constant was chosen to be small, i.e. $F_S \ll F_0$, following the idea of Ref. *Talà et al. (2019)* that pilus-
 920 substrate attachment is stabilized for small pilus tension. Furthermore, we chose $\epsilon = 2$, i.e. pilus
 921 detachment at zero loads is three times faster than for a slip-bond model. Fixing $E_0 = 32$ kPa [ob-
 922 tained from fitting the force-independent model (see Appendix 1-figure 1a)], the theoretical curves
 923 with the force-dependent off-rate constant were fitted using a least square fit in the parameter V_{max} .
 924 The catch-bond behavior captures qualitatively better the velocities at low rigidities but neither
 925 slip-bond nor catch-bond seem to perform better than the simple analytical force-independent
 926 detachment model for medium and high rigidities.

Appendix 2: Influence of bacterial motility on the onset of biofilm verticalization

927
928

A. Simple kinetic model

929

930

931

932

933

934

935

936

937

938

As described in the main text, we propose a simple kinetic model to capture the 2D to 3D transition of bacteria in growing microcolonies over time, i.e. we assume that colony verticalization results from a competition between bacterial division and motility, rather than from a competition between adhesion forces between bacteria or between bacteria and the substrate. We thus assume that there is no strong difference in the binding energy of a cell to the substrate as a function of its rigidity, and that this energy is slightly higher than that of binding to another cell. Bacteria thus prefer adhering to the substrate in all cases but can easily adhere to other cells if needed. Based on this assumption, we consider two key features of surface colonization to describe the 2D to 3D transition:

939

940

- Growth: initially, at time $t = 0$, one bacterium is attached to the surface. The number of bacteria N grows exponentially with time as:

$$N(t) = e^{\frac{t}{t_0}}. \quad (S.27)$$

941

942

943

944

945

946

947

The characteristic time scale, t_0 , accounts both for the growth and for the occasional detachment of bacteria from the surface. *De novo* attachment of bacteria to the surface is neglected. Furthermore, t_0 is assumed to be constant over time and across the different surfaces.

- Movement: bacteria explore the surface with a characteristic velocity V_{CM} and perform a random walk (we consider time and length scales larger than the persistence length/time of bacterial twitching motion). These displacements result in a spreading of the colony over a characteristic area $a(t)$ following a diffusive process:

$$a(t) = a_0 + \alpha V_{CM} t \quad (S.28)$$

948

949

where a_0 is the area of one bacterium and α is a phenomenological parameter related to the properties of the random walk.

950

951

952

953

From the two equations above, it is clear that the number of bacteria attached to the surface grows faster than the size of the corresponding colony. Therefore, at a critical time t_c corresponding to a critical number of bacteria N_c on the substrate, the area available to bacteria for spreading on the surface will be completely occupied. i.e. $a_0 N_c = a_0 N(t_c) = a(t_c)$ and thus

$$N_c = 1 + \gamma V_{CM} \ln(N_c) \quad (S.29)$$

954

955

956

957

where we have substituted $\ln(N_c)$ for t_c on the *r.h.s.* of Eq. (S.29) and $\gamma = \alpha t_0/a_0$. Solving this equation permits to obtain N_c as a function of V_{CM} and one unknown parameter, γ . Note that when $V_{CM} = 0$, a situation in which the bacteria do not move at all, the 2D to 3D transition occurs at the first division, i.e. as soon as $N_c > 1$.

958

959

960

961

962

963

964

965

966

967

968

It should be noted that here, just as V_{CM} is a characteristic velocity and not the mean speed of the bacteria (see main text, Fig. 3A), that the characteristic area $a(t)$ accessible to the bacteria in the colony at time t is not necessarily equal to the whole colony area: first because of their finite center-of-mass velocity V_{CM} ; secondly, because the local density may restrict their movement and the accessible surface. This effect is difficult to quantify because the fluctuations of density inside the colony area may be, depending on V_c , much greater than the ones encountered in the case of the Brownian diffusion of particles. Indeed, some bacteria remain static while others explore the surface extensively (main text, Fig. 3E). Another reason is that upon division, the two daughter cells are touching and there is hence a systematic fluctuation of density upon division. Therefore the area accessible for bacteria is rather an effective measure, which cannot be directly derived from

969 microscopic diffusion processes only. While other expressions could be used, this one is the sim-
 970 plest that can be proposed and matches our experimental data sufficiently well. One justification
 971 is that the underlying assumption that the velocity of bacteria is not affected by the local density
 972 (retaining the linear scaling of $a(t)$ with V_{CM}) is justified in the assessed situation where groups of
 973 closed-packed bacteria never exceed 5-8 cells before the 2D to 3D transition occurs. However, as
 974 a comparison, sub- and super-linear scalings will be compared with experimental data in the next
 975 section.

976
 977 To further analyze the microscopic meaning of γ , we note that it is the inverse of a velocity and
 978 is related to the compactness of the colony, with higher values indicating a sparser distribution
 979 of bacteria with a lesser probability that growing/twitching bacteria will encounter several others
 980 and move to 3D because of local crowding. However it is misleading to compare it to values that
 981 could be derived from random walks with persistence because of the above-mentioned discrep-
 982 ancy between the colony area and the area accessible to bacteria for further spreading. Relating γ
 983 to experimentally measured quantities on the cell movement would require a detailed analysis of
 984 the cell density fluctuations on the surface which is beyond the scope of this paper.

985 **B. Comparison of experimental data with the model**

986 All available data from which characteristic velocities were extracted (main text, Fig. 3B) were anal-
 987 ysed and included, with the exception of one data point on glass due to the presence of an air
 988 bubble on the surface before the onset of the 2D→3D transition. The characteristic velocities for
 989 each experiment and each rigidity were taken from Fig. 3B. The characteristic number of bacteria
 990 N_c per colony was estimated as follows.

- 991 • First, for low- and medium-rigidity surfaces (2.7 kPa, 6.1 kPa and 18.5 kPa), colony formation
 992 from isolated bacteria was monitored over time until the 2D to 3D transition occurs. The
 993 number of bacteria on the surface stemming from the initial isolated bacteria were then
 994 counted, and the count for all the colonies were averaged to calculate N_c . In addition, the
 995 average number of colonies forming in the observed area up to that point was also measured.
- 996 • For higher-rigidity surfaces, the movement of bacteria is too large to keep track of all bacteria
 997 stemming from the same progenitor as they mix or leave the field of view, while others are
 998 incoming. As a result, N_c was calculated by counting the total number of bacteria in the field
 999 of view at the time of the onset of the 2D to 3D transition, and dividing this number by the
 1000 estimated number of colonies as measured on low-rigidity surfaces. It should be noted that
 1001 in this case, the simple model presented above is not valid as it considers only one isolated
 1002 colony, and can be expected to yield overestimated values of N_c . Furthermore, our evaluation
 1003 method of the number of colonies in the field of view may be prone to error so we used a
 1004 "blind" evaluation procedure performed before the count of bacteria in the field of view, to
 1005 avoid possible biases. A change of 1 (compared to a mean value around 4) in the number
 1006 of colonies used to normalise the total number of bacteria provides a good estimate of the
 1007 error bars on each individual data point, and is comparable to the spread of the data points
 1008 (see Appendix 2-figure 1). When several surfaces of the same rigidity have been measured in
 1009 one experiment, the different N_c values are averaged.

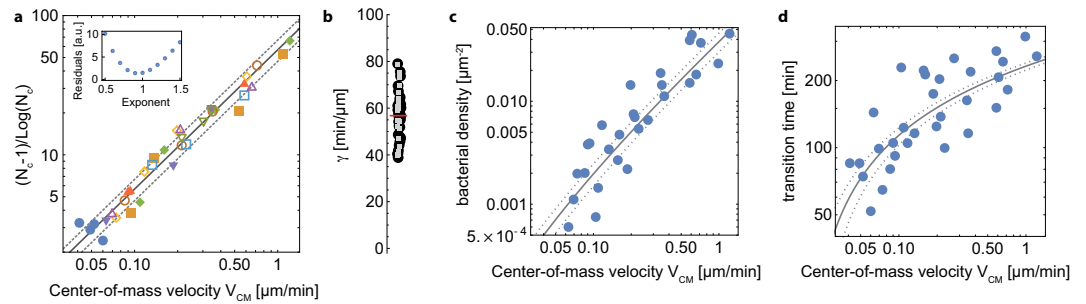
1010 The above cited procedure produced one doublet (V_{CM} , N_c) for each rigidity of each experiment.

1011 To match our simple model with the experimental data, Eq. (S.29) can be used to calculate N_c
 1012 as a function of V_{CM} for a given value of γ . However, a direct fit of the experimental data is difficult
 1013 as there is no analytical solution to Eq. (S.29). Instead, an experimental value of γ was calculated
 1014 from each experimental point using the expression

$$\gamma_{exp} = \frac{N_c - 1}{V_{CM} \ln(N_c)} \quad (S.30)$$

1015 An average experimental value is then calculated, along with a standard deviation, $\langle \gamma_{exp} \rangle = 56.8$
 1016 $\text{min} \cdot \mu\text{m}^{-1}$ and $\delta\gamma = 11.2 \text{ min} \cdot \mu\text{m}^{-1}$.

1017



Appendix 2-figure 1: (a) comparison between the experimental data (markers) and the kinetic model (lines). Blue dots are data obtained with the pili-deficient mutant *pilA*: Tn5. Inset, residual of the fit of all the experimental data points as a function of the exponent value for V_{CM} , indicating that the best fit is achieved for a value of or close to 1. (b) γ_{exp} values for all data points (black disks) and their average (red line). Gray squares are data points with $v_0 < 2 \mu\text{m} \cdot \text{min}^{-1}$, showing a similar distribution and thus ruling out a significant bias at high velocities. (c) same dataset as in a but the surface density at the transition is plotted; (d) same dataset as in a but the time at the transition is plotted. The same model is used to describe the data, but converted into the proper quantities.

1018 Appendix 2-figure 1a shows the experimental data $(N_c - 1)/\text{Log}(N_c)$ as a function of V_{CM} (each
 1019 marker corresponds to a different experiment), and the corresponding theoretical straight lines
 1020 with slopes $\langle \gamma_{exp} \rangle$ (solid line), and $\langle \gamma_{exp} \rangle \pm 1$ standard deviation (dotted lines). To assess the de-
 1021 viation from the curve at high velocities, $\langle \gamma_{exp} \rangle$ was also calculated from all data points with $v_0 <$
 1022 $2 \mu\text{m} \cdot \text{min}^{-1}$ but the change in the value is minimal ($58.2 \text{ min} \cdot \mu\text{m}^{-1}$ instead of $56.8 \text{ min} \cdot \mu\text{m}^{-1}$, see
 1023 Appendix 2-figure 1b).

1024 Our strongest assumption in this modelling is the expression of $a(t)$ as a function of V_{CM} [Eq. (S.28)]:
 1025 an obvious *a posteriori* evidence for its correctness is that the derived equation fits our data well
 1026 over more than one decade in velocity. To strengthen our point, however, we have also calculated
 1027 similar curves using an exponent for V_{CM} ranging from 0.5 to 1.5 (steps of 0.1, Appendix 2-figure
 1028 1a, inset): the comparison with experimental data indicates that reasonable agreement is only
 1029 obtained for exponent values between 0.8 and 1.1, at most.

1030 Finally we would like to point out that the data do not collapse as well when plotting the density
 1031 of bacteria, or the time of the 2D \rightarrow 3D transition (Appendix 2-figures 1c and 1d). A likely explana-
 1032 tion is that the initial number of bacteria on the surface varies between different datasets, a bias
 1033 that is cancelled when plotting the number of bacteria instead of the density or the time at the
 1034 onset of the transition. The same model is used with the same average parameter and spread,
 1035 but converted into the proper quantities: for the density, the curves in Appendix 2-figure 1a are
 1036 multiplied by the average number of colonies per observed area (3 colonies), and divided by the
 1037 image area ($26121 \mu\text{m}^2$); for the transition time, the logarithm of the number of bacteria per colony
 1038 at the transition is multiplied by the typical growth time of the number of bacteria on the surface
 1039 ($\sim 40 \text{ min}$). This time incorporates both the division time ($\sim 30 \text{ min}$) and the departure of a fraction
 1040 of the bacteria from the surface.

1041 References

- 1042 **Abidine Y**, Laurent VM, Michel R, Duperray A, Palade LI, Verdier C. Physical properties of polyacrylamide gels
 1043 probed by AFM and rheology. *Europhys Lett*. 2015 FEB; 109(3). doi: {10.1209/0295-5075/109/38003}.
- 1044 **Aoudia N**, Rieu A, Briandet R, et al. Biofilms of *Lactobacillus plantarum* and *Lactobacillus fermentum*: Effect
 1045 on stress responses, antagonistic effects on pathogen growth and immunomodulatory properties. *Food*
 1046 *Microbiol*. 2016; 53(Pt A):51-59. <https://doi.org/10.1016/j.fm.2015.04.009>.

- 1047 **Arganda-Carreras I**, Kaynig V, Rueden C, Eliceiri KW, Schindelin J, Cardona A, Sebastian Seung H. Trainable
1048 Weka Segmentation: a machine learning tool for microscopy pixel classification. *Bioinformatics*. 2017;
1049 33(15):2424–2426.
- 1050 **Armbruster CR**, Lee CK, Parker-Gilham J, de Anda J, Xia A, Zhao K, Murakami K, Tseng BS, Hoffman LR, Jin F,
1051 Harwood CS, Wong GC, Parsek MR. Heterogeneity in surface sensing suggests a division of labor in *Pseu-*
1052 *domonas aeruginosa* populations. *eLife*. 2019; 8.
- 1053 **Beamish JA**, Zhu J, Kottke-Marchant K, Marchant RE. The effects of monoacrylated poly(ethylene glycol) on the
1054 properties of poly(ethylene glycol) diacrylate hydrogels used for tissue engineering. *J Biomed Mater Res A*.
1055 2010 FEB; 92A(2):441–450. doi: {10.1002/jbm.a.32353}.
- 1056 **Beaussart A**, Baker AE, Kuchma SL, El-Kirat-Chatel S, O'Toole GA, Dufrêne YF. Nanoscale adhesion forces of
1057 *Pseudomonas aeruginosa* type IV pili. *ACS nano*. 2014; 8(10):10723–10733.
- 1058 **Björnham O**, Axner O. Catch-Bond Behavior of Bacteria Binding by Slip Bonds. *Biophysical Journal*. 2010 Sep;
1059 99(5):1331–1341. <https://doi.org/10.1016/j.bpj.2010.06.003>, doi: 10.1016/j.bpj.2010.06.003.
- 1060 **Boucher HW**, Talbot GH, Bradley JS, et al. Bad bugs, no drugs: no ESKAPE! An update from the Infectious
1061 Diseases Society of America. *Clin Infect Dis*. 2009; 48(1):1–12. <https://doi.org/10.1086/599017>.
- 1062 **Chang CY**. Surface sensing for biofilm formation in *Pseudomonas aeruginosa*. *Front Microbiol*. 2018; 8:2671.
- 1063 **Conrad JC**, Gibiansky ML, Jin F, Gordon VD, Motto DA, Mathewson MA, Stopka WG, Zelasko DC, Shrout JD, Wong
1064 GCL. Flagella and Pili-Mediated Near-Surface Single-Cell Motility Mechanisms in *P. aeruginosa*. *Biophys J*.
1065 2011 APR 6; 100(7):1608–1616. doi: {10.1016/j.bpj.2011.02.020}.
- 1066 **Cont A**, Rossy T, Al-Mayyah Z, Persat A. Biofilms deform soft surfaces and disrupt epithelia. *eLife*. 2020; 9.
1067 <https://doi.org/10.7554/elife.56533>.
- 1068 **Cont A**, Vermeil J, Persat A. Material Substrate Physical Properties Control *Pseudomonas aeruginosa* Biofilm
1069 Architecture. *mBio*. 2023; p. e03518–22. <https://journals.asm.org/doi/abs/10.1128/mbio.03518-22>, doi:
1070 10.1128/mbio.03518-22.
- 1071 **Cornforth DM**, Dees JL, Ibberson CB, Huse HK, Mathiesen IH, Kirketerp-Møller K, Wolcott RD, Rum-
1072 baugh KP, Bjarnsholt T, Whiteley M. *Pseudomonas aeruginosa* transcriptome during human infection.
1073 *Proc Natl Acad Sci USA*. 2018; 115(22):E5125–E5134. <https://www.pnas.org/content/115/22/E5125>, doi:
1074 10.1073/pnas.1717525115.
- 1075 **Cowles KN**, Gitai Z. Surface association and the MreB cytoskeleton regulate pilus production, localization and
1076 function in *Pseudomonas aeruginosa*. *Mol Microbiol*. 2010 Jun; 76(6):1411–1426.
- 1077 **Craig L**, Forest KT, Maier B. Type IV pili: dynamics, biophysics and functional consequences. *Nature Reviews*
1078 *Microbiology*. 2019; 17(7):429–440. [https://doi.org/10.1038/s41579-019-](https://doi.org/10.1038/s41579-019-0195-4)
1079 0195-4.
- 1080 **DeLeon S**, Clinton A, Fowler H, Everett J, Horswill AR, Rumbaugh KP. Synergistic interactions of *Pseudomonas*
1081 *aeruginosa* and *Staphylococcus aureus* in an in vitro wound model. *Infection and Immunity*. 2014 Nov;
1082 82(11):4718–4728.
- 1083 **Dötsch A**, Eckweiler D, Schniederjans M, et al. The *Pseudomonas aeruginosa* transcriptome in planktonic cul-
1084 tures and static biofilms using RNA sequencing. *PLoS One*. 2012; 7(2):e31092. [https://journals.plos.org/](https://journals.plos.org/plosone/article?id=10.1371/journal.pone.0031092)
1085 [plosone/article?id=10.1371/journal.pone.0031092](https://journals.plos.org/plosone/article?id=10.1371/journal.pone.0031092).
- 1086 **Dufrêne YF**. Sticky microbes: forces in microbial cell adhesion. *Trends Microbiol*. 2015; 23(6):376–382. <https://doi.org/10.1016/j.tim.2015.01.011>.
- 1088 **Dufrêne YF**, Persat A. Mechanomicrobiology: how bacteria sense and respond to forces. *Nat Rev Microbiol*.
1089 2020; 18:1–14.
- 1090 **Duvernoy MC**, Mora T, Ardré M, et al. Asymmetric adhesion of rod-shaped bacteria controls microcolony
1091 morphogenesis. *Nat comm*. 2018; 9(1):1–10. <https://doi.org/10.1038/s41467-018-03446-y>.
- 1092 **Evans E**. Probing the relation between forceâlifetimedand chemistry in single molecular bonds. Annual review
1093 of biophysics and biomolecular structure. 2001; 30(1):105–128.

- 1094 **Furukawa S**, Kuchma SL, O'Toole GA. Keeping Their Options Open: Acute versus Persistent Infections. *Journal*
1095 *of Bacteriology*. 2006 Feb; 188(4):1211–1217.
- 1096 **Gellatly SL**, Hancock REW. *Pseudomonas aeruginosa* : new insights into pathogenesis and host de-
1097 fenses . *Pathogens and Disease*. 2013 04; 67(3):159–173. <https://doi.org/10.1111/2049-632X.12033>, doi:
1098 [10.1111/2049-632X.12033](https://doi.org/10.1111/2049-632X.12033).
- 1099 **Grant MAA**, Waclaw B, Allen RJ, Cicuta P. The role of mechanical forces in the planar-to-bulk transition in
1100 growing *Escherichia coli* microcolonies. *J Roy Soc Inter*. 2014 AUG 6; 11(97). doi: {10.1098/rsif.2014.0400}.
- 1101 **Islam S**, Krachler AM. Mechanosensing regulates virulence in *Escherichia coli* O157:H7. *Gut Microbes*. 2016;
1102 7(1):63–67. <https://doi.org/10.1080/19490976.2015.1121365>.
- 1103 **Jackson K**, Starkey M, Kremer S, Parsek M, Wozniak D. Identification of psl, a locus encoding a potential ex-
1104 opolysaccharide that is essential for *Pseudomonas aeruginosa* PAO1 biofilm formation. *J Bacteriol*. 2004 JUL;
1105 186(14):4466–4475. doi: {10.1128/JB.186.14.4466-4475.2004}.
- 1106 **Jacobs MA**, Alwood A, Thaipisuttikul I, Spencer D, Haugen E, Ernst S, Will O, Kaul R, Raymond C, Levy R, Chun-
1107 Rong L, Guenther D, Bovee D, Olson MV, Manoil C. Comprehensive transposon mutant library of *Pseu-*
1108 *domonas aeruginosa*. *Proc Natl Acad Sci USA*. 2003; 100(24):14339–14344. [https://www.pnas.org/content/](https://www.pnas.org/content/100/24/14339)
1109 [100/24/14339](https://www.pnas.org/content/100/24/14339), doi: [10.1073/pnas.2036282100](https://doi.org/10.1073/pnas.2036282100).
- 1110 **Jin F**, Conrad JC, Gibiansky ML, Wong GCL. Bacteria use type-IV pili to slingshot on surfaces. *Proc*
1111 *Natl Acad Sci USA*. 2011; 108(31):12617–12622. <https://www.pnas.org/content/108/31/12617>, doi:
1112 [10.1073/pnas.1105073108](https://doi.org/10.1073/pnas.1105073108).
- 1113 **Koch MD**, Black ME, Han E, Shaevitz JW, Gitai Z. *Pseudomonas aeruginosa* distinguishes
1114 surfaces by stiffness using retraction of type IV pili. *Proceedings of the National Academy of*
1115 *Sciences*. 2022; 119(20):e2119434119. <https://www.pnas.org/doi/abs/10.1073/pnas.2119434119>, doi:
1116 [10.1073/pnas.2119434119](https://doi.org/10.1073/pnas.2119434119).
- 1117 **Koch MD**, Fei C, Wingreen NS, Shaevitz JW, Gitai Z. Competitive binding of independent extension and retraction
1118 motors explains the quantitative dynamics of type IV pili. *Proceedings of the National Academy of Sciences*.
1119 2021 Feb; 118(8):e2014926118. <https://doi.org/10.1073/pnas.2014926118>, doi: [10.1073/pnas.2014926118](https://doi.org/10.1073/pnas.2014926118).
- 1120 **Kramers HA**. Brownian motion in a field of force and the diffusion model of chemical reactions. *Physica*. 1940
1121 Apr; 7(4):284–304. [https://doi.org/10.1016/s0031-8914\(40\)90098-2](https://doi.org/10.1016/s0031-8914(40)90098-2), doi: [10.1016/s0031-8914\(40\)90098-2](https://doi.org/10.1016/s0031-8914(40)90098-2).
- 1122 **Kühn MJ**, Talà L, Inclan YF, Patino R, Pierrat X, Vos I, Al-Mayyah Z, Macmillan H, Negrete J, Engel JN, Persat A.
1123 Mechanotaxis directs *Pseudomonas aeruginosa* twitching motility. *Proc Natl Acad Sci USA*. 2021; 118(30).
1124 <https://www.pnas.org/content/118/30/e2101759118>, doi: [10.1073/pnas.2101759118](https://doi.org/10.1073/pnas.2101759118).
- 1125 **Kuik J**, Vincent S, Leeftang B, Kroon-Batenburg LMJ, Kamerling J. Conformational analysis in aqueous solu-
1126 tion and estimation of the persistence length of exopolysaccharides produced by *Lactobacillus helveticus*
1127 Lh59 and *Streptococcus macedonicus* Sc136. *Canadian Journal of Chemistry*. 2011 02; 84:730–742. doi:
1128 [10.1139/v06-055](https://doi.org/10.1139/v06-055).
- 1129 **Landau LD**, Lifschitz EM. *Theory of Elasticity*, vol. 7 of *Theoretical Physics*. 3 ed. Butterworth Heinemann; 2004.
- 1130 **Laventie BJ**, Jenal U. Surface sensing and adaptation in bacteria. *Annu Rev Microbiol*. 2020; 74:735–760.
- 1131 **Laventie BJ**, Sangermani M, Estermann F, Manfredi P, Planes R, Hug I, Jaeger T, Meunier E, Broz P, Jenal U. A
1132 Surface-Induced Asymmetric Program Promotes Tissue Colonization by *Pseudomonas aeruginosa*. *Cell Host*
1133 *Microbe*. 2018 Dec; p. 1–20.
- 1134 **Leighton TL**, Buensuceso RNC, Howell PL, Burrows LL. Biogenesis of *Pseudomonas aeruginosa* type IV pili and
1135 regulation of their function. *Environmental Microbiology*. 2015 Nov; 17(11):4148–4163.
- 1136 **Liu Y**, Yang CH, Li J. Influence of extracellular polymeric substances on *Pseudomonas aeruginosa* trans-
1137 port and deposition profiles in porous media. *Environ Sci Technol*. 2007 JAN 1; 41(1):198–205. doi:
1138 {10.1021/es061731n}.
- 1139 **Livingston J**, Spero MA, Lonergan ZR, Newman DK. Visualization of mRNA Expression in *Pseudomonas aerug-*
1140 *inosa* Aggregates Reveals Spatial Patterns of Fermentative and Denitrifying Metabolism. *bioRxiv*. 2022;
1141 <https://www.biorxiv.org/content/early/2022/03/12/2022.03.11.484052>, doi: [10.1101/2022.03.11.484052](https://doi.org/10.1101/2022.03.11.484052).

- 1142 **Lu S**, Giuliani M, Harvey H, LL B, Wickham R, Dutcher J. Nanoscale Pulling of Type IV Pili Reveals Their Flexibility
1143 and Adhesion to Surfaces over Extended Lengths of the Pili. . 2015; 108(12):2865–2875.
- 1144 **Ma L**, Lu H, Sprinkle A, Parsek MR, Wozniak DJ. *Pseudomonas aeruginosa* PSI is a galactose- and mannose-rich
1145 exopolysaccharide. J Bacteriol. 2007 NOV; 189(22):8353–8356. doi: {10.1128/JB.00620-07}.
- 1146 **Maier B**, Wong GCL. How Bacteria Use Type IV Pili Machinery on Surfaces. Trends Microbiol. 2015; 23(12):775–
1147 788. <https://doi.org/10.1016/j.tim.2015.09.002>.
- 1148 **Mann EE**, Wozniak DJ. *Pseudomonas* biofilm matrix composition and niche biology. FEMS Microbiol Rev. 2012
1149 JUL; 36(4):893–916. doi: {10.1111/j.1574-6976.2011.00322.x}.
- 1150 **Marathe R**, Meel C, Schmidt NC, Dewenter L, Kurre R, Greune L, Schmidt MA, Müller MJI, Lipowsky R,
1151 Maier B, Klumpp S. Bacterial twitching motility is coordinated by a two-dimensional tug-of-war with di-
1152 rectional memory. Nature Communications. 2014 May; 5(1). <https://doi.org/10.1038/ncomms4759>, doi:
1153 10.1038/ncomms4759.
- 1154 **Marko JF**, Siggia ED. Statistical mechanics of supercoiled DNA. Physical Review E. 1995; 52(3):2912.
- 1155 **Merz AJ**, So M, Sheetz MP. Pilus retraction powers bacterial twitching motility. Nature. 2000; 407(6800):98–102.
1156 <https://doi.org/10.1038/35024105>.
- 1157 **Moradali MF**, Ghods S, Rehm BHA. *Pseudomonas aeruginosa* Lifestyle: A Paradigm for Adaptation, Survival,
1158 and Persistence. Front Cell Infect Microbiol. 2017; 7:39. <https://doi.org/10.3389/fcimb.2017.00039>.
- 1159 **Moran PA**. Notes on continuous stochastic phenomena. Biometrika. 1950; 37(1/2):17–23.
- 1160 **O'Neal L**, Baraquet C, Suo Z, Dreifus JE, Peng Y, Raivio TL, Wozniak DJ, Harwood CS, Parsek MR. The Wsp sys-
1161 tem of *Pseudomonas aeruginosa* links surface sensing and cell envelope stress. Proceedings of the
1162 National Academy of Sciences. 2022; 119(18):e2117633119. [https://www.pnas.org/doi/abs/10.1073/pnas.](https://www.pnas.org/doi/abs/10.1073/pnas.2117633119)
1163 [2117633119](https://www.pnas.org/doi/abs/10.1073/pnas.2117633119), doi: 10.1073/pnas.2117633119.
- 1164 **Orazi G**, O'Toole GA, Dunman P. *Pseudomonas aeruginosa* Alters *Staphylococcus aureus* Sensitivity to Vancomycin
1165 in a Biofilm Model of Cystic Fibrosis Infection. mBio. 2017; 8(4):e00873–17. [https://journals.asm.org/doi/abs/](https://journals.asm.org/doi/abs/10.1128/mBio.00873-17)
1166 [10.1128/mBio.00873-17](https://journals.asm.org/doi/abs/10.1128/mBio.00873-17), doi: 10.1128/mBio.00873-17.
- 1167 **O'Toole GA**, Kolter R. Flagellar and twitching motility are necessary for *Pseudomonas aeruginosa* biofilm de-
1168 velopment. Mol Microbiol. 1998 Oct; 30(2):295–304.
- 1169 **Pang Z**, Raudonis R, Glick BR, Lin TJ, Cheng Z. Antibiotic resistance in *Pseudomonas aerug-*
1170 *inosa*: mechanisms and alternative therapeutic strategies. Biotechnology Advances. 2019;
1171 37(1):177–192. <https://www.sciencedirect.com/science/article/pii/S0734975018301976>, doi:
1172 <https://doi.org/10.1016/j.biotechadv.2018.11.013>.
- 1173 **Pereverzev YV**, Prezhdo OV, Forero M, Sokurenko EV, Thomas WE. The Two-Pathway Model for the Catch-Slip
1174 Transition in Biological Adhesion. Biophysical Journal. 2005 Sep; 89(3):1446–1454. [https://doi.org/10.1529/](https://doi.org/10.1529/biophysj.105.062158)
1175 [biophysj.105.062158](https://doi.org/10.1529/biophysj.105.062158), doi: 10.1529/biophysj.105.062158.
- 1176 **Persat A**, Inclan YF, Engel JN, et al. Type IV pili mechanochemically regulate virulence factors in *Pseudomonas*
1177 *aeruginosa*. Proc Natl Acad Sci USA. 2015; 112(24):7563–7568. <https://doi.org/10.1073/pnas.1502025112>.
- 1178 **Persat A**, Nadell CD, Kim MK, et al. The Mechanical World of Bacteria. Cell. 2015; 161(5):988–997. <https://doi.org/10.1016/j.cell.2015.05.005>.
- 1180 **Reichhardt C**, Wong C, Passos da Silva D, Wozniak DJ, Parsek MR. CdrA Interactions within the *Pseudomonas*
1181 *aeruginosa* Biofilm Matrix Safeguard It from Proteolysis and Promote Cellular Packing. MBio. 2018 Sep; 9(5).
- 1182 **Robert P**, Benoliel AM, Pierres A, Bongrand P. What is the biological relevance of the specific bond properties
1183 revealed by single-molecule studies? Journal of Molecular Recognition: An Interdisciplinary Journal. 2007;
1184 20(6):432–447.
- 1185 **Rodesney CA**, Roman B, Dhamani N, Cooley BJ, Touhami A, Gordon VD. Mechanosensing of shear by *Pseu-*
1186 *domonas aeruginosa* leads to increased levels of the cyclic-di-GMP signal initiating biofilm development.
1187 Proc Natl Acad Sci USA. 2017 JUN 6; 114(23):5906–5911. doi: {10.1073/pnas.1703255114}.
- 1188 **Rybtke MT**, Borlee BR, Murakami K, et al. Fluorescence-based reporter for gauging cyclic di-GMP levels in
1189 *Pseudomonas aeruginosa*. Appl Environ Microbiol. 2012; 78(15):5060–5069.

- 1190 **Saha N**, Monge C, Dulong V, et al. Influence of Polyelectrolyte Film Stiffness on Bacterial Growth. *Biomacromol.*
1191 2013; 14(2):520–528. <https://doi.org/10.1021/bm301774a>.
- 1192 **Sahoo PK**, Janissen R, Monteiro MP, et al. Nanowire Arrays as Cell Force Sensors To Investigate Adhesin-
1193 Enhanced Holdfast of Single Cell Bacteria and Biofilm Stability. *Nano Letters.* 2016; 16(7):4656–4664. <https://doi.org/10.1021/acs.nanolett.6b01998>.
1194
- 1195 **Sens P**. Rigidity sensing by stochastic sliding friction. *EPL (Europhysics Letters).* 2013; 104(3):38003.
- 1196 **Shen Y**, Siryaporn A, Lecuyer S, et al. Flow Directs Surface-Attached Bacteria to Twitch Upstream. *Biophys J.*
1197 2012; 103(1):146–151. <https://doi.org/10.1016/j.bpj.2012.05.045>.
- 1198 **Shrout JD**, Tolker-Nielsen T, Givskov M, Parsek MR. The contribution of cell-cell signaling and motility to bacte-
1199 rial biofilm formation. *MRS Bull.* 2011 May; 36(5):367–373.
- 1200 **Simsek AN**, Braeutigam A, Koch MD, Shaevitz JW, Huang Y, Gompper G, Sabass B. Substrate-rigidity dependent
1201 migration of an idealized twitching bacterium. *Soft Matter.* 2019; 15(30):6224–6236. [https://doi.org/10.1039/](https://doi.org/10.1039/c9sm00541b)
1202 [c9sm00541b](https://doi.org/10.1039/c9sm00541b), doi: 10.1039/c9sm00541b.
- 1203 **Siryaporn A**, Kuchma SL, O'Toole GA, Gitai Z. Surface attachment induces *Pseudomonas aeruginosa* virulence.
1204 *Proc Natl Acad Sci U S A.* 2014 Nov; 111(47):16860–16865.
- 1205 **Skerker JM**, Berg HC. Direct observation of extension and retraction of type IV pili. *Proc Natl Acad Sci USA.*
1206 2001; 98(12):6901–6904.
- 1207 **Song F**, Ren D. Stiffness of Cross-Linked Poly(Dimethylsiloxane) Affects Bacterial Adhesion and Antibiotic Sus-
1208 ceptibility of Attached Cells. *Langmuir.* 2014; 30(34):10354–10362. <https://doi.org/10.1021/la502029f>, doi:
1209 10.1021/la502029f.
- 1210 **Song F**, Wang H, Sauer K, Ren D. Cyclic-di-GMP and oprF Are Involved in the Response of *Pseudomonas aerug-*
1211 *inosa* to Substrate Material Stiffness during Attachment on Polydimethylsiloxane (PDMS). *Front Microbiol.*
1212 2018; 9:110. <https://doi.org/10.3389/fmicb.2018.00110>.
- 1213 **Song F**, Wang H, Sauer K, Ren D. Cyclic-di-GMP and oprF Are Involved in the Response of *Pseudomonas aerugi-*
1214 *nosa* to Substrate Material Stiffness during Attachment on Polydimethylsiloxane (PDMS). *Frontiers in Microbi-*
1215 *ology.* 2018; 9. <https://www.frontiersin.org/article/10.3389/fmicb.2018.00110>, doi: 10.3389/fmicb.2018.00110.
- 1216 **Stoodley P**, Sauer K, Davies D, Costerton J. Biofilms as complex differentiated communities. *Annu Rev Microbiol.*
1217 2002; 56:187–209. doi: {10.1146/annurev.micro.56.012302.160705}.
- 1218 **Talà L**, Fineberg A, Kukura P, Persat A. *Pseudomonas aeruginosa* orchestrates twitching motility by sequential
1219 control of type IV pili movements. *Nat Microbiol.* 2019; 4(5):774–780.
- 1220 **Thevenaz P**, Ruttimann UE, Unser M. A pyramid approach to subpixel registration based on intensity. *IEEE*
1221 *transactions on image processing.* 1998; 7(1):27–41.
- 1222 **Tinevez JY**, Perry N, Schindelin J, Hoopes GM, Reynolds GD, Laplantine E, Bednarek SY, Shorte SL, Eliceiri KW.
1223 TrackMate: An open and extensible platform for single-particle tracking. *Methods.* 2017; 115:80–90.
- 1224 **Tse JR**, Engler AJ. Preparation of hydrogel substrates with tunable mechanical properties. *Curr Protoc Cell Biol.*
1225 2010; 47:10.16. <https://doi.org/10.1002/0471143030.cb1016s47>.
- 1226 **Valentini M**, Filloux A. Biofilms and Cyclic di-GMP (c-di-GMP) Signaling: Lessons from *Pseudomonas aerugi-*
1227 *nosa* and Other Bacteria. *Journal of Biological Chemistry.* 2016 Jun; 291(24):12547–12555.
- 1228 **Wadhwa N**, Berg HC. Bacterial motility: machinery and mechanisms. *Nature Reviews Microbiology.* 2022 Mar;
1229 20(3):161–173.
- 1230 **Webster SS**, Mathelié-Guinlet M, Verissimo AF, Schultz D, Viljoen A, Lee CK, Schmidt WC, Wong GCL, Dufrêne
1231 YF, O'Toole GA, Kline KA. Force-Induced Changes of PilY1 Drive Surface Sensing by *Pseudomonas*
1232 *aeruginosa*. *mBio.* 2022; 13(1):e03754–21. <https://journals.asm.org/doi/abs/10.1128/mbio.03754-21>, doi:
1233 10.1128/mbio.03754-21.
- 1234 **Williams T**, Kelley C, many others, Gnuplot 5.2: an interactive plotting program; 2019. <http://gnuplot.sourceforge.net/>.
1235
- 1236 **Zhao K**, Tseng BS, Beckerman B, et al. Psl trails guide exploration and microcolony formation in *Pseudomonas*
1237 *aeruginosa* biofilms. *Nature.* 2013; 497(7449):388–391. <https://doi.org/10.1038/nature12155>.